ACS NANO

www.acsnano.org

ARTICLE

Enhancing Glioblastoma Immunotherapy with Integrated Chimeric Antigen Receptor T Cells through the Re-Education of Tumor-Associated Microglia and Macrophages

Nianci Zhu, Sijia Chen, Yu Jin, Meng Wang, Luyao Fang, Lingjing Xue, Dexiang Hua, Ziyao Zhang, Meng Jia, Meixi Hao,* and Can Zhang*

Cite This: https://doi.org/10.1021/acsnano.4c00050

Read Online

ACCESS | Metrics & More | Article Recommendations | Supporting Information

ABSTRACT: Glioblastoma (GBM) is an aggressive brain cancer that is highly resistant to treatment including chimeric antigen receptor (CAR)-T cells. Tumor-associated microglia and macrophages (TAMs) are major contributors to the immunosuppressive GBM microenvironment, which promotes tumor progression and treatment resistance. Hence, the modulation of TAMs is a promising strategy for improving the immunotherapeutic efficacy of CAR-T cells against GBM. Molecularly targeting drug pexidartinib (PLX) has been reported to re-educate TAMs toward the antitumorigenic M1-like phenotype. Here, we developed a cell−drug integrated technology to reversibly conjugate PLX-containing liposomes (PLX-Lip) to CAR-T cells and establish tumor-responsive integrated CAR-T cells (PLX-Lip/AZO-T cells) as a combination therapy for GBM. We used a mouse model of GBM to show that PLX-Lip was stably maintained on the surface of PLX-Lip/AZO-T cells in circulation and these cells could transmigrate across the blood−brain barrier and deposit PLX-Lip at the tumor site. The uptake of PLX-Lip by TAMs effectively re-educated them into the M1-like phenotype, which in turn boosted the antitumor function of CAR-T cells. GBM tumor growth was completely eradicated in 60% of the mice after receiving PLX-Lip/AZO-T cells and extended their overall survival time beyond 50 days; in comparison, the median survival time of mice in other treatment groups did not exceed 35 days. Overall, we demonstrated the successful fusion of CAR-T cells and small-molecule drugs with the cell−drug integrated technology. These integrated CAR-T cells provided a superior combination strategy for GBM treatment and presented a reference for the construction of integrated cell-based drugs.

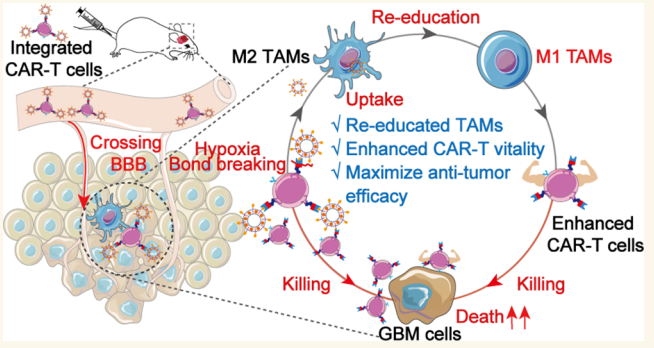

KEYWORDS: *glioblastoma, CAR-T cells, re-educated TAMs, blood−brain barrier, cell−drug integrated technology*

INTRODUCTION

Glioblastoma (GBM) is the most common and fatal malignant brain tumor in adults. Even when treated aggressively with conventional surgery combined with radiotherapy and temozolomide chemotherapy, the median survival of patients with GBM is less than 2 years.[1−3] Cancer immunotherapy has brought newfound hope to patients with GBM.[4−6] Among the available modes of cancer immunotherapy, those involving the manipulation and engineering of antitumor effector cells, particularly chimeric antigen receptor (CAR)-T cell therapy, have been most successful in treating GBM.[7,8] Many early clinical trials have shown that CAR-T cells can transmigrate across the blood−brain barrier (BBB) and thus exert a therapeutic effect on GBM.[9,10] However, the five-year overall survival rates of patients with GBM receiving CAR-T cell therapy remain below 10%.[2] Increasing evidence highlights the vital role of the immunosuppressive tumor microenvironment (TME) in promoting treatment tolerance.[4,11] This barrier must be overcome to fully unleash the antitumor capabilities of

Received: January 2, 2024
Revised: March 31, 2024
Accepted: April 5, 2024

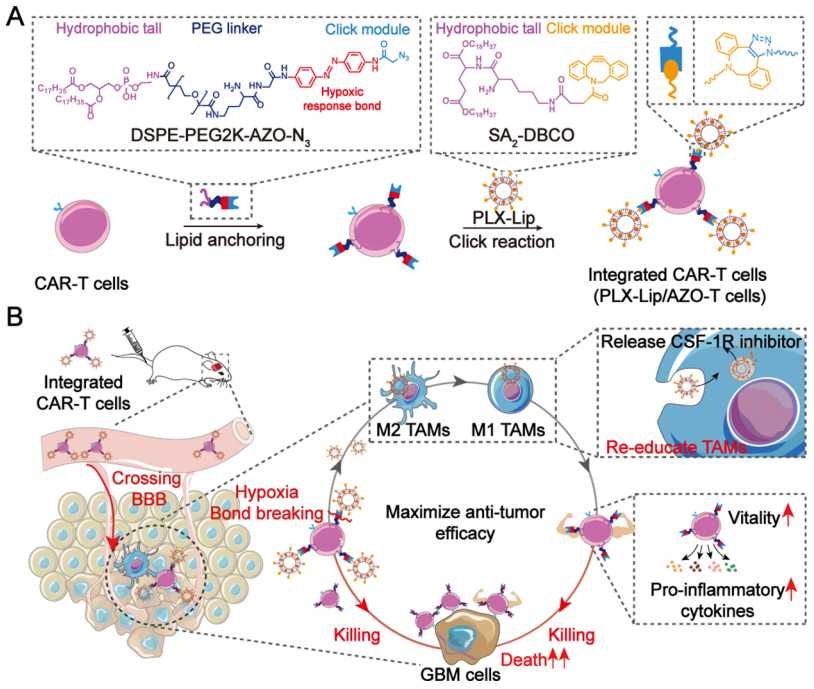

Figure 1. Integrated CAR-T cells (PLX-Lip/AZO-T cells) re-educate tumor-associated microglia and macrophages and enhance glioblastoma immunotherapy. (A) Schematic illustration of the cell−drug integrated technology to construct the PLX-Lip/AZO-T cells. An azide-bearing lipid was inserted into the lipid bilayer of the CAR-T cell membrane, which contains the hypoxia-responsive moiety azobenzene (AZO). The subsequent click reaction between the azide on the CAR-T cell surface and the DBCO-containing liposomal PLX (PLX-Lip) contributes to the generation of the integrated CAR-T cells (PLX-Lip/AZO-T cells). (B) Schematic mechanism of PLX-Lip/AZO-T cells for enhancing glioblastoma immunotherapy. PLX-Lip/AZO-T cells re-educated TAMs to the M1-like antitumorigenic phenotype by effectively crossing the BBB and releasing PLX-Lip at the GBM site. The alleviation of TAMs-mediated immunosuppression in turn increased the immune potency and therapeutic effect of the integrated CAR-T cells.

immune effector cells. As a major cellular component of the immunosuppressive microenvironment of GBM, tumor-associated microglia and macrophages (TAMs), which include peripheral macrophages derived from hematopoietic stem cells (HSCs) and brain-resident microglia derived from immature yolk sac progenitors, are a key driver of both immunosuppression and therapy resistance in GBM.[12,13] Given that 30−50% of cells in a GBM mass are TAMs, there are intriguing possibilities for re-educating these cells to function as antitumor effector cells.[14] Such an approach promises to boost the therapeutic efficacy of CAR-T cell therapy for GBM.

It has been reported that microglia and macrophages are recruited to the GBM tumor and develop a tumor-promoting phenotype primarily through signaling molecules produced by GBM cells, stromal fibroblasts, and the macrophages themselves.[15] These signaling molecules include transforming growth factor-β (TGF-β), macrophage colony-stimulating factor-1 (CSF-1), monocyte chemotactic protein-1 (MCP-1, also called CCL-2), interleukin-4 (IL-4), immune complexes recognized by receptors targeting the Fc portion of immunoglobulin G (FcγRs), and complement.[15] Among them, CSF-1, released by GBM cells, acts as a microglia and macrophages chemoattractant and converts microglia and macrophages into protumorigenic M2-like microglia and macrophages. These M2-like microglia and macrophages in turn release epidermal growth factor (EGF), which induces glioma-promoting activity and stimulates the growth and invasion of GBM cells.[14,16] Thus, interfering with CSF-1 signaling represents a potential strategy for targeting the TAMs-mediated regulation of GBM growth. Several studies of preclinical GBM models have shown that CSF-1R inhibition induces the apoptosis of M2-like microglia and macrophages and repolarization toward M1-like microglia and macrophages.[17,18] Moreover, in animal models, CSF-1R inhibition improved the efficacy of several immunotherapeutic modalities, including immune checkpoint blockade and adoptive T-cell therapy.[18]

Pexidartinib (PLX3397, PLX), a marketed small-molecule CSF-1R inhibitor (CSF-1Ri), has been reported to re-educate TAMs toward the antitumorigenic, M1 phenotype.[19] Blockade of the CSF-1/CSF-1R axis by PLX decreased the expression of protumorigenic genes in TAMs and upregulated the expression of genes associated with antigen presentation and lymphocyte activation.[20] Moreover, PLX reshaped the immune microenvironment and induced positive crosstalk between TAMs and T cells, thereby maintaining a network of antitumor responses.[21] However, the results of a phase II clinical trial showed that although PLX was well tolerated, it had little therapeutic effect in patients with GBM (NCT01349036). This disappointing result was likely due to the insufficient accumulation and persistence of PLX in the GBM mass after oral administration.[22]

Therefore, we would like to develop a cell−drug integrated technology that integrates the CAR-T cells and PLX to construct integrated CAR-T cells for the combination treatment of GBM. This therapeutic strategy of combining PLX with CAR-T cells might contribute to an increase in antitumor efficacy and potentially reduce the nonspecific distribution of PLX in healthy tissues, alleviating any toxicity associated with the administration of higher doses of the drug. Meanwhile, PLX shed from CAR-T cells would be taken up by TAMs to remodel the GBM microenvironment and improve

https://doi.org/10.1021/acsnano.4c00050
ACS Nano XXXX, XXX, XXX−XXX

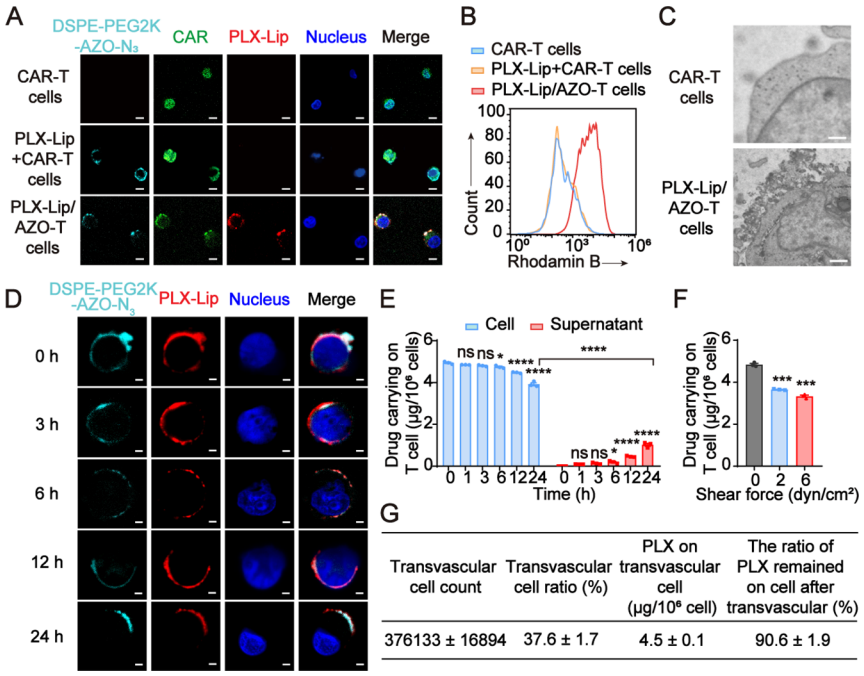

G

Transvascular cell count	Transvascular cell ratio (%)	PLX on transvascular cell (μg/10⁶ cell)	The ratio of PLX remained on cell after transvascular (%)
376133 ± 16894	37.6 ± 1.7	4.5 ± 0.1	90.6 ± 1.9

Figure 2. Successful construction of integrated CAR-T cells (PLX-Lip/AZO-T cells). (A) Confocal images of PLX-Lip/AZO-T cells. Cy5-tagged DSPE-PEG2k-AZO-N_3 (cyan), GFP expressed by CAR (green), Rhodamine B-labeled PLX-Lip (red), T-cell nucleus (blue); scale bar, 5 μm. (B) Flow cytometric assay of PLX-Lip conjugated to the PLX-Lip/AZO-T cells. (C) Biology transmission electron microscope images of PLX-Lip/AZO-T cells; scale bar, 2 μm. (D) Confocal images of the stability of liposomes (red) retained on the surface of CAR-T cells at different times. Scale bar, 2 μm. (E) Drug-loading stability of PLX-Lip/AZO-T cells. (F) Drug-loading stability of PLX-Lip/AZO-T cells under different blood shear forces. (G) Transvascular ability and stability of PLX-Lip/AZO-T cells. Data represent the mean ± SEM (n = 3). *$P \leq 0.05$; ***$P \leq 0.001$; ****$P \leq 0.0001$; ns, not significant; determined by two-way ANOVA with Tukey's correction in E, or one-way ANOVA with Tukey's correction in (F).

the efficacy of the CAR-T cells. Hence, the aim of the present study was to develop an integrated form of GBM therapy that combines the antitumor properties of CAR-T cells and PLX. To this end, we construct tumor-responsive integrated CAR-T cells by the cell−drug integrated technology. Specifically, PLX was reversibly conjugated to the surface of CAR-T cells via a lipid-containing hypoxia-responsive moiety because hypoxia is a key feature of the GBM microenvironment.[23,24]

As shown in Figure 1A, this cell−drug integrated technology was a two-step approach involving lipid anchoring and a click reaction. Briefly, the hypoxia-responsive moiety azobenzene (AZO)[25] was introduced into an azide-bearing lipid, which was inserted into the lipid bilayer of the CAR-T cell membrane. Then, the integrated CAR-T cells (PLX-Lip/AZO-T cells) were generated via a click reaction[26] between the azide on the CAR-T cell surface and the DBCO-containing liposomal PLX (PLX-Lip). We showed that PLX-Lip cells were retained on the surface of CAR-T cells in circulation, could cross the BBB, and were released from CAR-T cells in the hypoxic GBM microenvironment. Subsequently, the uptake of free PLX-Lip by TAMs led to their re-education toward the antitumorigenic phenotype, which in turn boosted the antitumor activity of the integrated CAR-T cells. Overall, integrated CAR-T cells based on the cell−drug integrated technology of combining CAR-T cells and PLX are expected to achieve the optimized CAR-T cell immunotherapy for GBM (Figure 1B). This study will provide a therapeutic strategy for combining cell drugs with small-molecule drugs and has great potential for rapid translation into clinical practice.

RESULTS AND DISCUSSION

Design and Construction of PLX-Lip/AZO-T Cells. The azide-bearing lipid (DSPE-PEG2K-AZO-N_3) containing AZO and complementary DBCO-derived lipid (SA_2-DBCO) were designed and synthesized (Figure S1); their structures were verified by proton nuclear magnetic resonance (^{1}H NMR, Figure S2). Under hypoxic conditions, the UV absorbance of AZO at 380 nm gradually decreased over time and almost completely disappeared at 9 h (Figure S3). This result indicates that, under hypoxic conditions, the AZO bond in DSPE-PEG2K-AZO-N_3 was rapidly cleaved and fully reduced within 9 h. Next, PLX-Lip were prepared using SA_2-DBCO and the film dispersion method; the resulting particles had an average diameter of 200 nm and a positive charge of +21 mV. The drug-loading efficiency (DL%) and entrapment efficiency (EE%) of PLX-Lip were 3.2 and 94.2%, respectively (Figure S4A,B). Transmission electron microscopy (TEM) showed that PLX-Lip had a uniform spheroid morphology (Figure S4C). In addition, PLX-Lip remained stable in vitro for 48 h under different conditions including T cell medium, physiological conditions (i.e., PBS), and serum-containing medium (to simulate conditions in the blood, Figure S5). Moreover, the GD2 CAR-T cells were constructed and characterized according to previous reports (Figure S6).[27]

Next, we generated the PLX-Lip/AZO-T cells by conjugating PLX-Lip to the GD2 CAR-T cells via the cell−drug integrated technology. We investigated a series of cellular anchor-click parameters, including anchor-click feeding concentrations and time. We found that during the anchoring of DSPE-PEG2K-AZO-N_3 to the membrane of CAR-T cells, the Cy5 fluorescent intensity of DSPE-PEG2K-AZO-N_3 on CAR-

https://doi.org/10.1021/acsnano.4c00050
ACS Nano XXXX, XXX, XXX−XXX

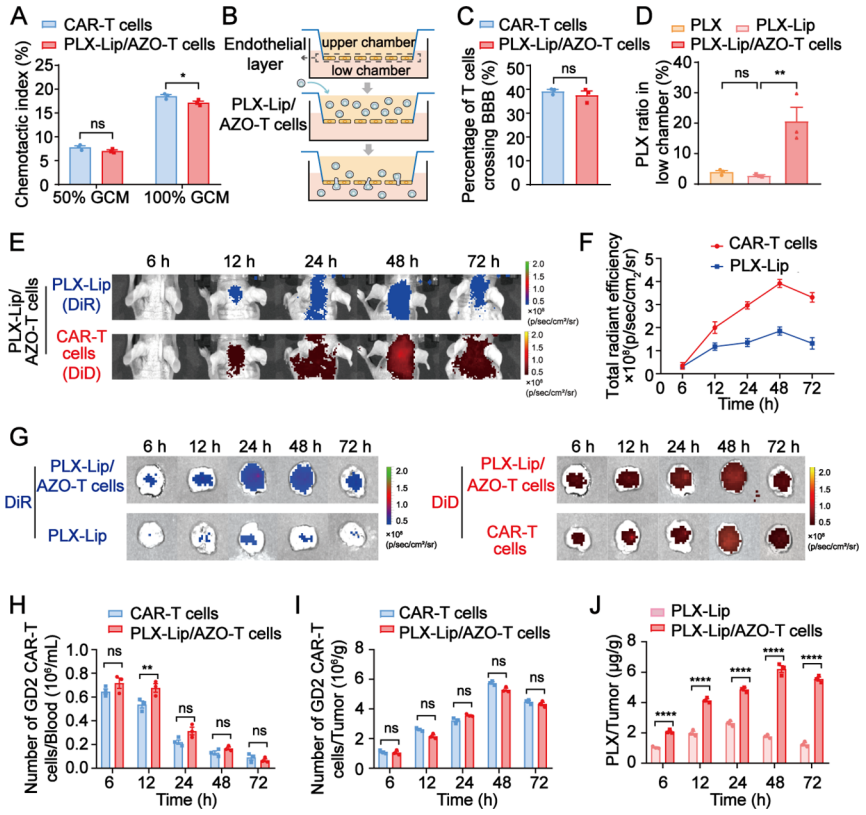

Figure 3. BBB-crossing and GBM-targeting capability of PLX-Lip/AZO-T cells. (A) Chemotaxis of PLX-Lip/AZO-T cells and CAR-T cells after incubation with GCM for 12 h. (B) Schematic representation of the trans-well assay for exploring the ability of crossing the BBB. (C) Transmigration of PLX-Lip/AZO-T cells and CAR-T cells after incubation with GCM for 12 h. (D) Quantification of the PLX in the trans-well low chamber after PLX, PLX-Lip, or PLX-Lip/AZO-T cells incubating with GCM for 12 h. The distribution (E) and quantitation (F) of PLX-Lip (DIR-labeled) and CAR-T cells (DID-labeled) of PLX-Lip/AZO-T cells after *i.v.* administration over time in the brain of GBM-bearing mice. (G) Distribution of PLX-Lip (DIR-labeled) and CAR-T cells (DID-labeled) of PLX-Lip/AZO-T cells in ex vivo glioma tissue after *i.v.* administration over time, with PLX-Lip (DIR-labeled) and CAR-T cells (DID-labeled) as controls. Flow cytometric analysis of the number of $CD3^+DID^+$CAR-T cells in the blood (H) and tumor (I), with CAR-T cells as a control. (J) Concentration of PLX accumulated in tumors over time after *i.v.* administration of PLX-Lip or PLX-Lip/AZO-T cells. Drug concentration was analyzed via HPLC. Data represent the mean ± SEM ($n = 3$). $^*P \le 0.05$; $^{**}P \le 0.01$; $^{****}P \le 0.0001$; ns, not significant; determined by student's unpaired *t* test in C, or one-way ANOVA with Tukey's correction in A and D, or two-way ANOVA with Tukey's correction in (H), (I), and (J).

T cells peaked when 18 μM DSPE-PEG2K-AZO-N_3 was coincubated with CAR-T cells for 10 min; notably, these conditions did not impact CAR-T cells viability (Figure S7). Having selected the best feeding concentration (18 μM) and time of DSPE-PEG2K-AZO-N_3 anchoring to the CAR-T cells (10 min), we subsequently optimized the click reaction conditions, including the concentration of PLX-Lip and the incubation time. To maximize the loading of PLX on CAR-T cells while ensuring cell viability, the concentration of PLX-Lip was set to 100 μg/mL PLX, and the incubation time was set to 45 min, corresponding to peak Cy5 fluorescence of DSPE-PEG2K-AZO-N_3 and peak rhodamine fluorescence of PLX-Lip on the CAR-T cells. Under the optimized condition, the loading of PLX on CAR-T cells was up to 4.6 μg of PLX per million cells (Figure S8).

To confirm that PLX-Lip cells were conjugated to the surface of CAR-T cells rather than adhering to them nonspecifically or taken up into the cytoplasm, the CAR-T cells anchored with DSPE-PEG2K-AZO-N_3 were incubated with DBCO-free liposomes (PLX-Lip+CAR-T cells) as a control. We then subjected the different types of CAR-T cells to confocal imaging, flow cytometry, and nanoparticle tracking analysis (NTA). Microscopic evaluation of the surface of PLX-Lip/AZO-T cells revealed that the Cy5 fluorescence of DSPE-PEG2K-AZO-N_3 was clearly colocalized with the rhodamine fluorescence of liposomes, whereas the colocalization of these signals was not observed in either PLX-Lip+CAR-T cells or CAR-T cells alone (Figure 2A). This result indicates that the click reaction between the azide and DBCO occurred successfully, meaning that the PLX-Lip cells were indeed conjugated to the CAR-T cell surface. Flow cytometry also showed that PLX-Lip/AZO-T cells had the highest fluorescence intensity among all the CAR-T cell groups, suggesting that most of the PLX-Lip were specifically conjugated to the CAR-T cell membrane (Figures 2B and S9). Moreover, we detected about 227 liposomes in each PLX-Lip/AZO-T cell; whereas the count of DBCO-free liposomes in each CAR-T cell was only 29. The comparison of these two values further illustrates that nearly all liposomes are conjugated onto the surface of CAR-T cells instead of being taken up or adhering to the cells (Figure S10). Taken together, these results indicate that the conjugation of PLX-Lip to the CAR-T cells was due to the successful anchoring of DSPE-PEG2K-AZO-N_3 in the cell membrane and subsequent click reaction rather than physical adhesion or cellular uptake. We next performed a biology transmission electron microscope to evaluate the morphology of PLX-Lip/AZO-T cells, which revealed the presence of liposomes on the surface of CAR-T cells (Figure 2C). Analysis

https://doi.org/10.1021/acsnano.4c00050
ACS Nano XXXX, XXX, XXX−XXX

of CAR-T cell function confirmed that the PLX-Lip/AZO-T cells had similar physiological activities to those of conventional CAR-T cells, including viability, proliferation, activation, ability to secrete multiple cytokines, and even cell membrane fluidity (Figure S11). These data suggest that the cell−drug integrated technology did not perturb the vital functions of CAR-T cells.

Next, we investigated the stability of the liposomes and PLX on the surface of the CAR-T cells. Confocal images showed that the fluorescence of liposomes was stable on the surface of CAR-T cells for up to 24 h under physiological conditions (Figure 2D). Moreover, high-performance liquid chromatography (HPLC) revealed that >80% of PLX was still stably sequestered on the CAR-T cell surface after 24 h of incubation in a T-cell expansion medium and serum-containing medium (Figures 2E and S12). These data indicated that PLX-Lip/AZO-T cells maintained fulfilling drug-loading stability in the storage environment and blood circulation. Even when subjected to the forces typically encountered in inflamed micro- and arterial blood vessels, >80% of the PLX-containing liposomes remained on the surface of CAR-T cells (Figure 2F). This result further indicates that PLX-Lip/AZO-T cells were able to retain their surface drug in circulation. Moreover, we found that >90% of PLX remained stably conjugated to PLX-Lip/AZO-T cells after they had crossed the vasculature (Figure 2G). Collectively, these results indicate that PLX-Lip/AZO-T cells exhibit excellent liposome and PLX stability, which should enable them to effectively accumulate drugs in the tumor site.

BBB-Crossing and GBM-Targeting Capability of PLX-Lip/AZO-T Cells. The BBB, which consists of continuous tight and adherent junctions between brain capillary endothelial cells, distinguishes the brain from other organs and protects it from inflammation and toxic substances.[11,28] At the same time, most therapeutic agents, even immune cells, are excluded from brain parenchyma due to the existence of BBB. Thus, the BBB is the main drug delivery bottleneck in the treatment of GBM.[29,30] However, the discovery of lymphatic vessels lining the dural sinuses has challenged the perception of the brain as an immune-privileged organ.[31,32] These vessels exchange fluid with the cerebral spinal fluid (CSF) surrounding the brain parenchyma, facilitating the trafficking of effector T cells into and out of the brain.[33] Numerous clinical practices have also reported the infiltration of CAR-T cells into the glioma site, confirming that CAR-T cells could penetrate the BBB and target GBM.[9,34] However, we needed to determine whether the PLX-Lip/AZO-T cells also had these capabilities.

Therefore, we first used GBM-cell-derived conditioned medium (GCM) to simulate the GBM microenvironment and investigated the ability of PLX-Lip/AZO-T cells to perform chemotaxis toward gliomas. The results showed that PLX-Lip/AZO-T cells and GD2 CAR-T cells displayed similar chemotactic abilities in a GCM-concentration-dependent manner (Figure 3A). Then, we constructed a trans-well model using endothelial cells to mimic the BBB in vitro (Figure 3B). Approximately 37.6% of the PLX-Lip/AZO-T cells transmigrated across the BBB, which was not significantly different from the percentage of CAR-T cells (39.2%) crossing the BBB (Figure 3C). In addition, when transported by PLX-Lip/AZO-T cells, >20% of the PLX crossed the BBB, while only 3.9% of free PLX would cross the BBB unaided (Figure 3D). Taken together, these findings show that the PLX-Lip/AZO-T cells displayed excellent ability to cross the BBB in vitro model, facilitating the accumulation of PLX in the tumor site.

To evaluate the ability of PLX-Lip/AZO-T cells to cross the BBB and target GBM in vivo, we established an orthotopic GBM-bearing mouse model. To this end, we injected human luciferase-expressing glioblastoma cells (LN-229-Luci cells) into the right frontal lobe of BALB/c nude mice. The fluorescence intensity of the mouse brain increased over time, confirming the successful construction of the orthotopic glioma model (Figure S13). Then, PLX-Lip/AZO-T cells, in which CAR-T cells and PLX-Lip were labeled with DID and DIR, respectively, were intravenously injected into the GBM-bearing mice. The DID and DIR signals were clearly observed in the mouse brain at 12 h after the intravenous administration of PLX-Lip/AZO-T cells (Figure 3E,F). The fluorescence intensities of both dyes increased simultaneously over time and peaked at 48 h, revealing that the PLX-Lip conjugated to the surface of CAR-T cells had successfully transmigrated across the BBB to reach the glioma site. At 72 h, a strong DID signal of PLX-Lip/AZO-T cells was still present in the brain, whereas the DIR signal of PLX-Lip gradually diminished (Figure 3G, left). Moreover, the DID signals of PLX-Lip/AZO-T cells and CAR-T cells in the brains of mice were similar over the 72 h monitoring period (Figure 3G, right). Taken together, these results suggest that PLX-Lip/AZO-T cells could pass through the BBB and promote the accumulation of PLX-Lip at the GBM site in vivo. In addition, we found that the adoptively transferred PLX-Lip/AZO-T cells and CAR-T cells were localized mainly to the liver and spleen. This pattern of localization could be attributed to the preferential homing of CAR-T cells to these organs, confirming that the cell−drug integrated technology did not affect the distribution of CAR-T cells in vivo (Figure S14).

To better understand the ability of PLX-Lip/AZO-T cells to carry PLX-Lip across the BBB, we further analyzed the biodistribution of the CAR-T cell component by flow cytometry and the PLX component by HPLC. We found that the distribution of PLX-Lip/AZO-T cells in blood was highly consistent with that of the GD2 CAR-T cells (Figures 3H and S15A). This finding further confirmed that the cell−drug integrated technology did not affect the distribution of CAR-T cells in vivo. We found similar numbers of PLX-Lip/AZO-T cells and CAR-T cells in the brain (Figures 3I and S15B). Moreover, these CAR-T cell populations exhibited similar dynamics, as a significant aggregation of PLX-Lip/AZO-T cells and CAR-T cells was detected in the brain at 12 h after injection (peaking at 48 h). These findings are consistent with those of the ex vivo imaging experiments. Meanwhile, the injection of PLX-Lip/AZO-T cells significantly increased the amount of PLX in the brain (versus PLX-Lip alone); at 48 h, the peak percentage of PLX in the brains of the PLX-Lip/AZO-T cell group was 3.5-fold higher than that of the PLX-Lip group. The results of the comparison suggested that the accumulation of PLX at the site of GBM was dramatically improved by the ability of PLX-Lip/AZO-T cells to transmigrate across the BBB (Figure 3J). Moreover, we showed that, after adoptive transfer, some of the PLX-Lip/AZO-T cells first homed to the spleen (peak of aggregation = 6 h) instead of directly to the GBM site; this behavior was consistent with that of CAR-T cells (Figure S16). Overall, our findings show that PLX-Lip/AZO-T cells retained the tumor chemotactic and BBB-crossing capabilities of their parent GD2 CAR-T cells; these valuable properties enabled PLX to attain the same

https://doi.org/10.1021/acsnano.4c00050
ACS Nano XXXX, XXX, XXX−XXX

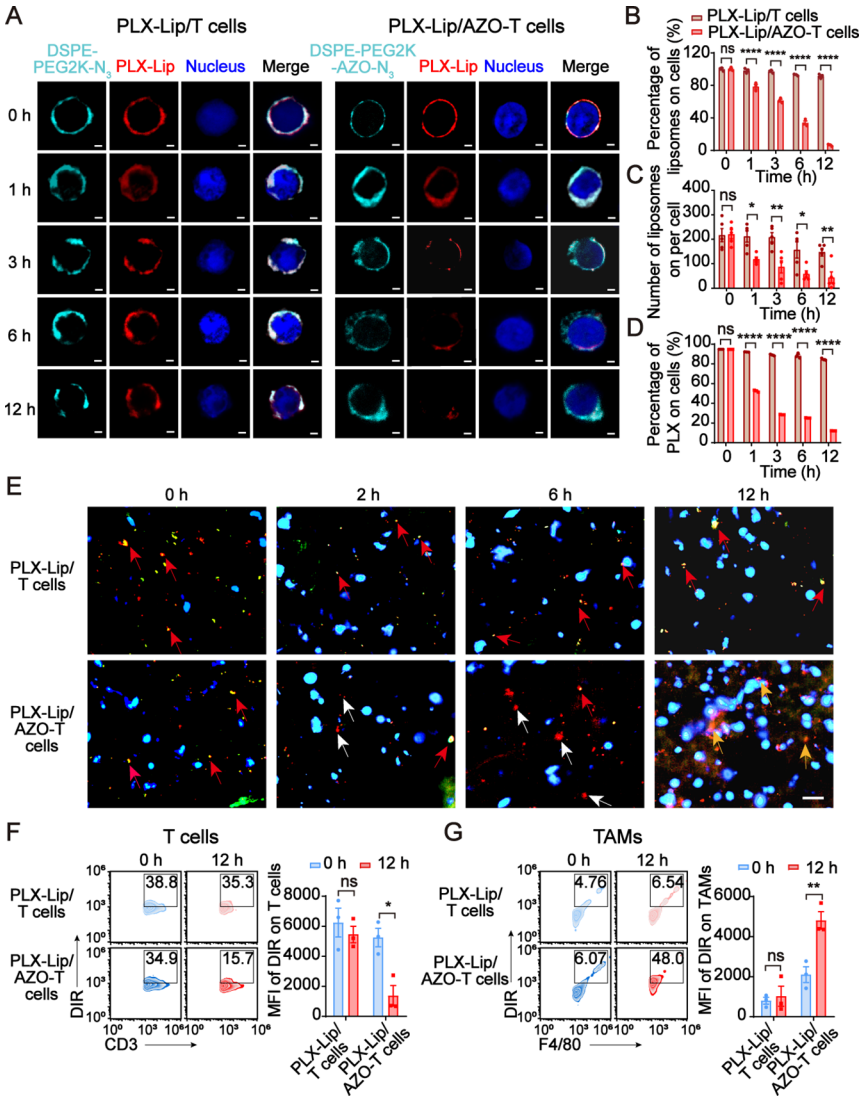

Figure 4. PLX-Lip released from PLX-Lip/AZO-T cells under hypoxic conditions. (A) Confocal microscopy images of PLX-Lip/T cells and PLX-Lip/AZO-T cells under hypoxic conditions at different times. Cy5-tagged DSPE-PEG2k-N_3 (cyan), GFP expressed by CAR (green), Rhodamine B-labeled PLX-Lip (red), and T-cell nucleus (blue; scale bar, 2 μm). Determination of PLX-Lip remained on the surface of PLX-Lip/AZO-T cells under hypoxic conditions over time by flow cytometry (B, n = 3) and NTA (C, n = 5), with PLX-Lip/T cells as a control. (D) HPLC analysis of PLX remained on the surface of PLX-Lip/AZO-T cells under hypoxic conditions over time, with PLX-Lip/T cells as a control (n = 3). (E) Distribution of PLX-Lip, CAR-T cells, and TAMs in glioma tissue at different times after *i.v.* administration of PLX-Lip/T cells or PLX-Lip/AZO-T cells by Nano Zoomer S60. DIR-labeled PLX-Lip (red, highlighted with white arrow), GFP of CAR-T cells (green), Cy3-tagged TAM (brown), cell nucleus (blue), the colocalization of liposomes with CAR-T cells (yellow fluorescence signal, highlighted with red arrow), and the localization of liposomes with TAMs (orange fluorescence signal, highlighted with yellow arrow). Scale bar, 20 μm. (F) Flow cytometric analysis of the release of PLX-Lip from CAR-T cells in glioma tissue at different times after *i.v.* administration of PLX-Lip/T cells or PLX-Lip/AZO-T cells. (G) Flow cytometric analysis of the uptake of PLX-Lip by TAMs in glioma tissue at different times after *i.v.* administration of PLX-Lip/T cells or PLX-Lip/AZO-T cells. Data represent the mean ± SEM (n = 3). *$P \leq 0.05$; **$P \leq 0.01$; ****$P \leq 0.0001$; ns, not significant; determined by two-way ANOVA with Tukey's correction.

biodistribution as the CAR-T cells and eventually enhanced the accumulation of PLX in GBM.

Hypoxia-Responsive Release of PLX-Lip from PLX-Lip/AZO-T Cells. The release of PLX-Lip in the glioma microenvironment and its subsequent uptake by TAMs are also necessary for the therapeutic effect of PLX-Lip/AZO-T cells. Having shown that PLX-Lip/AZO-T cells successfully crossed the BBB and carried PLX-Lip to the GBM site, we next evaluated the dynamics of PLX release and uptake by TAMs. By anchoring the AZO-free lipid (DSPE-PEG2K–N_3) onto the membranes of CAR-T cells and subsequent click reaction with PLX-Lip, we generated PLX-Lip/T cells that were not responsive to hypoxia (Figure S17). We then simulated the hypoxic microenvironment of GBM in vitro using a tri-gas incubator. Confocal microscopy images showed that the fluorescence of PLX-Lip on the surface of PLX-Lip/AZO-T cells rapidly disappeared and was barely visible after 12 h; by contrast, the surface of PLX-Lip/T cells maintained a strong fluorescent signal (Figure 4A). Flow cytometry revealed that >90% of the liposomes were detached from the PLX-Lip/AZO-T cells after 12 h of incubation in a hypoxic environment, while <10% of the liposomes were detached from the PLX-Lip/T cells (Figure 4B). Moreover, to further confirm that the PLX-Lip rather than PLX alone was shed from PLX-Lip/AZO-

https://doi.org/10.1021/acsnano.4c00050
ACS Nano XXXX, XXX, XXX−XXX

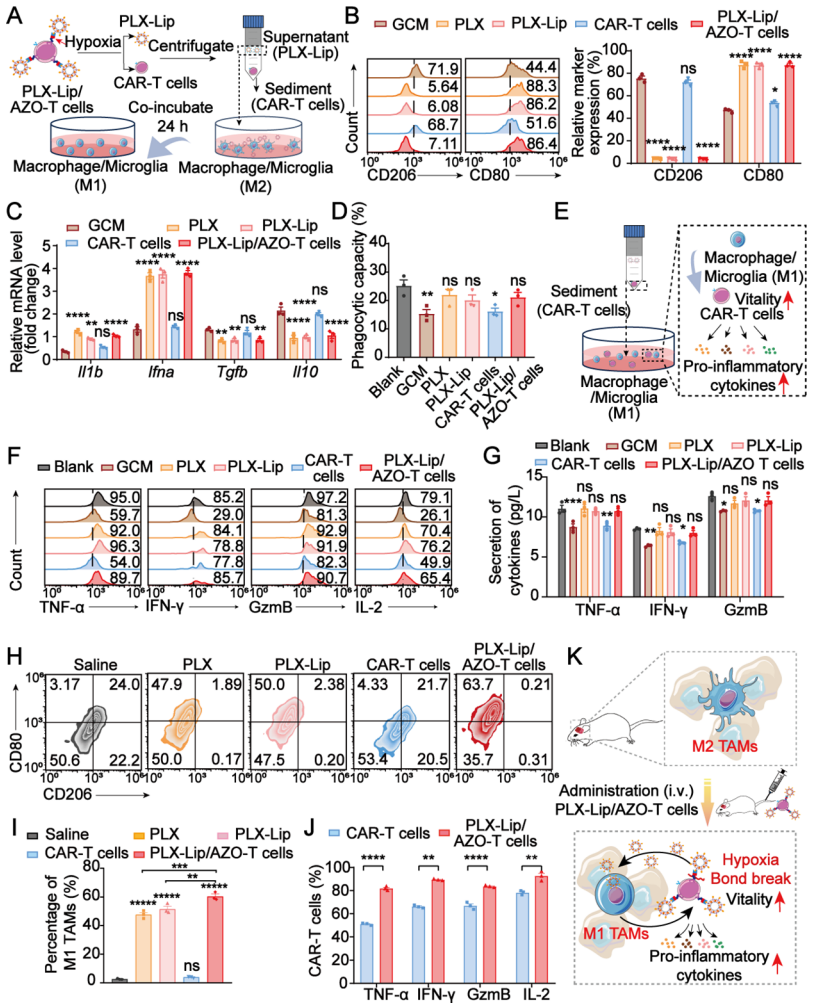

Figure 5. PLX-Lip/AZO-T cells re-educate TAMs. (A) Schematic of PLX-Lip/AZO-T cells releasing PLX-Lip in response to hypoxia and re-educating TAMs to assume the M1-like phenotype in vitro. (B) Flow cytometric analysis of CD206 and CD80 expression on microglia and macrophages after different treatments. (C) Relative mRNA levels of *Il1b, Tnfa, Tgfb,* and *Il10* in TAMs after different treatments. (D) Flow cytometric analysis of the proportion of F4/80$^+$ Hoechst$^+$ TAMs in all TAMs. (E) Schematic of the alleviation of immunosuppression microenvironment caused by TAMs and enhancement of CAR-T cells' antitumor efficacy through the re-education of TAMs toward M1-like phenotype. (F) Flow cytometric analysis of cytokine secretion of CAR-T cells incubated with TAMs after different treatments. (G) Cytokine release of CAR-T cells incubated with TAMs receiving different treatments by ELISA. (H and I) Flow cytometric analysis of the proportion of CD80$^+$CD206$^-$ TAMs in glioma. (J) Flow cytometric analysis of cytokine secretion of CAR-T cells in GBM after different treatments. (K) Schematic of PLX-Lip/AZO-T cells re-educating TAMs and enhancing the therapeutic effect of CAR-T cells. Data are represented as mean ± SEM; n = 3; *P < 0.05; **P < 0.01; ***P < 0.001; ****P < 0.0001; ns, not significant; determined by one-way ANOVA with Tukey's correction in (B), (D), (I), and (J), or two-way ANOVA with Tukey's correction in (C) and (G).

T cells in response to hypoxia, we evaluated the amount of PLX-Lip retained on the cell surface by NTA and the amount of PLX on the cells by HPLC. The amount of PLX-Lip on the PLX-Lip/AZO-T cells gradually decreased over time under the hypoxic environment, and nearly 80% of the liposomes were detached from CAR-T cells after 12 h, consistent with the confocal microscopy images and flow cytometric quantification (Figures 4C and S18). In addition, the amount of PLX released from the cells gradually increased with the extension of incubation time, and PLX was almost completely released at 12 h (Figure 4D). Taken together, these results indicate that PLX-Lip/AZO-T cells released PLX-Lip rather than PLX in response to the hypoxic environment and that PLX was only released after PLX-Lip detached from the cells and taken up by TAMs.

There is documentation that the intrinsic phagocytic properties and proximity to blood vessels of TAMs make it the predominant cell type to capture the nanoparticles extravagated from tumor blood vessels.[35] In view of the multiple cellular components of the GBM microenvironment and the phagocytic activity of tumor cells, we investigated the uptake ratio of PLX-Lip released from PLX-Lip/AZO-T cells between TAMs and glioma cells. Flow cytometric analysis displayed that the median fluorescent intensity (MFI) of RhoB-labeled PLX-Lip taken up by tumor association macrophages and microglia was 1.87-fold and 1.83-fold higher than that of glioma cells (Figure S19A). Moreover, it has been reported that the expression of CSF-1R in glioma cells enhances the proliferation of tumor cells and increases tumor malignancy, which could be alleviated by the inhibition of CSF-1R.[36,37] Therefore, we further detected the expression of Ki-67 in glioma cells after the coincubation with PLX-Lip released from PLX-Lip/AZO-T cells. As shown in Figure S19B, the uptake of PLX-Lip contributed to a 12.8% decrease

https://doi.org/10.1021/acsnano.4c00050
ACS Nano XXXX, XXX, XXX−XXX

in Ki-67 expression of glioma cells, implying that PLX could inhibit glioma cell proliferation and GBM growth. These data indicated that even if part of PLX-Lip is taken up by glioma cells, it can exert an inhibitory effect on GBM growth, aligning with our goal.

To further confirm that PLX-Lip/AZO-T cells enhanced the uptake of PLX-Lip by TAMs at the GBM site, GBM-bearing mice were randomly divided into two groups and injected intravenously with PLX-Lip/T cells or PLX-Lip/AZO-T cells. The PLX-Lip cells conjugated to the surface of the CAR-T cells were labeled with DIR. After the injection of PLX-Lip/AZO-T cells, the yellow fluorescence signal formed by the colocalization of the red fluorescent liposomes and green fluorescent CAR-T cells gradually disappeared in glioma tissues (Figure 4E). Meanwhile, the red fluorescence of liposomes gradually colocalized with the brown fluorescence of TAMs to form an orange fluorescent signal. Moreover, in the PLX-Lip/T cell group of mice, the red fluorescence of liposomes persistently colocalized with the green fluorescence of CAR-T cells in the glioma tissues (Figure 4E). Together, these findings suggest that PLX-Lip/AZO-T cells released PLX-Lip in response to the hypoxic GBM microenvironment and that these PLX-Lip were subsequently taken up by TAMs. Flow cytometric analysis also showed that >70% of the PLX-Lip were detached from CAR-T cells at 12 h after PLX-Lip/AZO-T cells infiltration, which was 5.8-fold higher than that of PLX-Lip/T cells (Figure 4F). Moreover, the uptake of PLX-Lip by TAMs was 4.7-fold higher in the PLX-Lip/AZO-T cell group than in the PLX-Lip/T cell group (Figure 4G). Collectively, these results suggest that PLX-Lip cells were rapidly released from PLX-Lip/AZO-T cells in the hypoxic microenvironment of GBM and were assimilated by TAMs as intended.

Re-education of Tumor-Associated Microglia and Macrophages by PLX-Lip/AZO-T Cells. We next sought to determine whether the PLX-Lip/AZO-T cells were capable of re-educating TAMs in the GBM microenvironment. We began by exploring the re-education of TAMs via PLX-Lip/AZO-T cells in vitro. To this end, we activated and polarized primary macrophages and microglia extracted from the bone marrow and brains of mice toward the M2-like phenotype to mimic TAMs (Figure S20A). The in vitro-generated TAMs exhibited high levels of purity (82.1% for macrophages and 83.5% for microglia) and CD206 (a marker of M2-like TAMs) expression (Figure S20B,C). The PLX-Lip/AZO-T cells were split into their PLX-Lip and CAR-T cell components under hypoxic conditions. After incubating M2-like TAMs with supernatant from PLX-Lip/AZO-T cells (PLX-Lip) for 24 h, their expression of CD206 and CD80 (M1-like phenotypic marker) was analyzed by flow cytometry (Figure 5A). The results showed that all the treated groups involving PLX decreased CD206 expression and increased CD80 expression on TAMs; moreover, there was no significant variation in the expression of these markers between the PLX-Lip/AZO-T cells-, PLX-, and PLX-Lip-treated groups, indicating that PLX-Lip/AZO-T cells could re-educate TAMs to assume the M1-like phenotype (Figures 5B and S21). qPCR analysis revealed that the expression of antitumor genes, including interleukin 1 beta (*Il1b*) and interferon-alpha (*Ifna*), in TAMs treated with PLX-Lip/AZO-T cells, was significantly upregulated compared with that of untreated M2-like TAMs (Figure 5C). Conversely, the expression of pro-tumor genes, including *Tgfb* and interleukin 10 (*Il10*), decreased after PLX-Lip/AZO-T cell treatment, confirming the TAM-re-educating capability of the PLX-Lip/AZO-T cells.

It has been reported that while M1-like TAMs engulf tumor cells, M2-like TAMs do not.[38] Having shown that PLX-Lip/AZO-T cells successfully re-educated TAMs from the M2-like to the M1-like phenotype, we next showed that the phagocytic capacity of TAMs was indeed significantly increased after treatment with PLX, PLX-Lip, or PLX-Lip/AZO-T cells (Figures 5D and S22A). We then confirmed that the ability of PLX-Lip/AZO-T cells to re-educate TAMs in vitro was comparable with that of PLX or PLX-Lip, confirming that the TAMs re-education was caused by the payload drug PLX. In addition, it has been reported that M1-like phenotypic TAMs exert a direct tumor-killing effect through the secretion of toxic effector molecules, such as toxic reactive oxygen species (ROS).[15,39] Therefore, we next explored the expression level of ROS in TAMs re-educated by PLX-Lip/AZO-T cells. The data showed that TAMs, re-educated from M2-like phenotype by the treatment of PLX-Lip/AZO-T cells, expressed higher levels of ROS than untreated M2-like TAMs (Figure S22B). Based on this, TAMs re-educated by PLX-Lip/AZO-T cells or untreated M2-like TAMs were coincubated with glioma cells (LN-229-luci cells), respectively, to investigate whether the TAMs reversed by PLX-Lip/AZO-T cells had direct tumor-killing ability through the secretion of ROS. As a result, glioma cells treated with TAMs re-educated by PLX-Lip/AZO-T cells exhibited a lower proliferation rate and a higher apoptosis rate (Figure S22C,D). These data suggest that M1-like TAMs, reversed through PLX-Lip/AZO-T cells, could exert a direct tumor-killing effect. More importantly, reversing the polarization of TAMs toward the M1-like phenotype attenuated the immunosuppression of CAR-T cells (Figure 5E). Owing to the exclusion of the important immunosuppressive factor, the vitality and pro-inflammatory cytokines secretion capacity of CAR-T cells were significantly increased (Figures 5F,G and S22E,F). Taken together, these data indicated that PLX-Lip/AZO-T cells reversed the polarization of TAMs toward the M1-like phenotype and displayed a combination effect of the direct tumor-killing effect of M1-like TAMs themselves and the potentiated CAR-T cells response.

The re-education effect of TAMs via PLX-Lip/AZO-T cells was further evaluated in vivo. After giving different formulations to GBM-bearing mice, we extracted and isolated TAMs and CAR-T cells from glioma tissue, before evaluating the phenotype of TAMs and the cytokine secretion capacity of CAR-T cells. Consistent with the in vitro results, formulations containing PLX significantly increased the proportion of M1-like TAMs ($CD80^+CD206^-$), demonstrating that PLX-Lip/AZO-T cells reprogrammed TAMs in vivo. In addition, PLX-Lip/AZO-T cell administration increased the proportion of intratumoral M1-like TAMs more than treatment with free PLX or PLX-Lip (Figure 5H,I). The results could be attributed to the cell−drug integrated technology that improves the accumulation of PLX at the site of GBM.

We found that PLX-Lip/AZO-T cells secreted higher levels of tumor necrosis factor-α (TNF-α), interferon-γ (IFN-γ), granzyme B (GzmB), and interleukin-2 (IL-2) than conventional tumor-infiltration CAR-T cells (Figures 5J and S23A). Moreover, PLX-Lip/AZO-T cells expressed lower levels of the inhibitory programmed death-1 (PD-1) receptor than GD2 CAR-T cells (Figure S23B), suggesting that the function of PLX-Lip/AZO-T cells was improved by alleviating the

https://doi.org/10.1021/acsnano.4c00050
ACS Nano XXXX, XXX, XXX−XXX

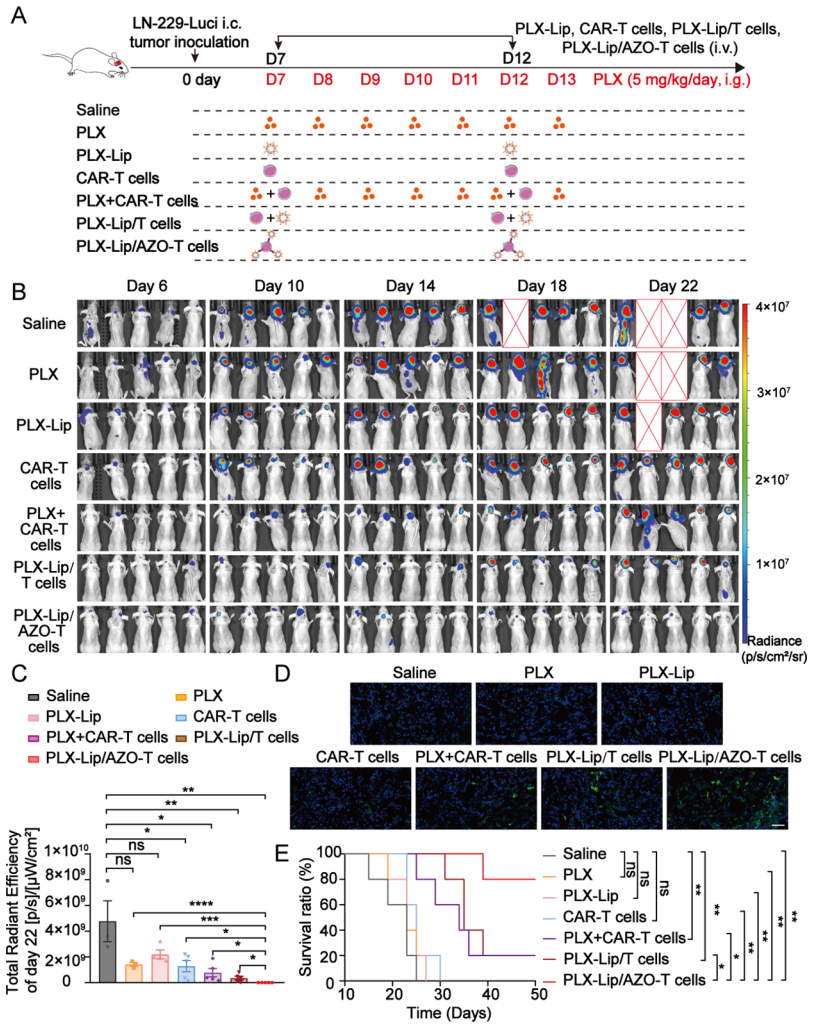

Figure 6. Antiglioma efficacy of PLX-Lip/AZO-T cells. (A) Schematic illustration of the experimental design. *i.c.*, intracranial. *i.v.*, intravenous. *i.g.*, intragastrical. In vivo bioluminescence images (B) and measurements of tumor size (C) in LN-229 tumor-bearing mice after different treatments. (D) TUNEL staining of tumor harvested from mice 24 h after the second dose on day 13. Scale bar, 50 μm. (E) Survival curves of mice receiving each treatment; n = 5 mice per group. Data are represented as mean ± SEM; *P < 0.05; **P < 0.01; ***P < 0.001; determined by one-way ANOVA with Tukey's correction in (C), or log-rank method with P values adjusted by Bonferroni correction in (E).

immunosuppressive effect of M2-like TAMs through their re-education.

In short, we have demonstrated that PLX-Lip/AZO-T cells successfully re-educated TAMs to the M1-like phenotype by effectively crossing the BBB and releasing PLX-Lip at the GBM site; the alleviation of TAMs-mediated immunosuppression in turn increased the immune potency of the PLX-Lip/AZO-T cells themselves (Figure 5K).

PLX-Lip/AZO-T Cells Administration Extends the Survival of GBM-Bearing Mice. Having demonstrated that PLX-Lip/AZO-T cells efficiently carried PLX-Lip to the hypoxic GBM site and re-educated TAMs, we next evaluated the antitumor efficacy of the PLX-Lip/AZO-T cells in vivo. GBM-bearing mice were randomly divided into seven groups: (1) Saline, (2) free PLX, (3) PLX-Lip, (4) CAR-T cells, (5) CAR-T cells plus free PLX (PLX+CAR-T cells), (6) PLX-Lip/T cells, and (7) PLX-Lip/AZO-T cells (Figure 6A). Depending on the group, the mice received two intravenous injections of PLX-Lip and CAR-T cells on days 7 and 12 after tumor implantation and daily intraperitoneal injection of free PLX from day 7. Tumor growth was monitored continuously by bioluminescence imaging after tumor implantation and treatment administration. We found that PLX-Lip/AZO-T cells significantly inhibited glioma growth, as evidenced by the fact that the tumor completely disappeared in three out of five mice. PLX+CAR-T cells and PLX-Lip/T cells delayed tumor progression, but not as effectively as PLX-Lip/AZO-T cells (Figure 6B,C). Meanwhile, the monotherapies (i.e., PLX, PLX-Lip, and CAR-T cells) showed limited therapeutic efficacy (Figure 6B,C). Tumors harvested from mice 24 h after the second treatment dose (i.e., on day 13) were subjected to the terminal deoxynucleotidyl transferase-mediated dUTP nick end labeling (TUNEL) assay to detect tumor cell apoptosis. The tumor cells in the PLX-Lip/AZO-T cells treatment group had the strongest TUNEL signal (Figure 6D), which aligned with the results of bioluminescence imaging. In addition, four out of the five mice receiving PLX-Lip/AZO-T cells survived for over 50 days; by contrast, the median survival time of mice from the other treatment groups was ≤35 days (Figure 6E). Together, these findings indicate that the PLX-Lip/AZO-T cells exerted the strongest antitumor effect among all the

https://doi.org/10.1021/acsnano.4c00050
ACS Nano XXXX, XXX, XXX−XXX

treatment modalities and significantly extended the survival time of GBM-bearing mice.

To evaluate the feasibility of using PLX-Lip/AZO-T cells in clinical practice, we next investigated their safety profile. We found that none of the treatment groups experienced a significant reduction in body weight or organ index changes (Figure S24A,B), compared with saline-treated mice. Pathological analysis of H&E staining also showed no evidence of significant tissue damage in any of the treatment groups (Figure S24C). The results of the blood biochemistry analysis showed that PLX-Lip/AZO-T cells did not reduce liver (alkaline phosphatase [ALP], alanine transaminase [ALT], and aspartate transaminase [AST], indicators of hepatic toxicity; Figure S25A−C) or kidney (lactate dehydrogenase [LDH], blood urea nitrogen [BUN], and creatinine [CRE], indicators of renal toxicity; Figure S25D−F) function. Mice treated with PLX-Lip/AZO-T cells also displayed no obvious increase in the systemic concentrations of interleukin-6 (IL-6), IL-10, or TNF-α, which are the major causal factors of the cytokine release syndrome (CRS), a serious adverse event associated with CAR-T therapy (Figure S25G−I). Overall, these findings suggest that PLX-Lip/AZO-T cells have a favorable safety profile and hold great potential for treating GBM in the clinic.

CONCLUSIONS

To date, the U.S. Food and Drug Administration (FDA) has approved six CAR-T cell products, all for the treatment of hematological malignancies[40]; meanwhile, there are no CAR-T cell products on the market for the treatment of solid tumors. Over 30 early clinical trials of CAR-T cells for GBM treatment have been launched worldwide. Given that GBM exhibits biological complexities as a brain tumor, CAR-T cell offers multiple therapeutic benefits over other treatments, such as chemotherapy with temozolomide and targeted therapy with bevacizumab.[41] On the one hand, the low level of tumor mutational load and deficiency of antigen presentation process undermine the efficacy of other immunotherapies against GBM.[42,43] While the application of CAR-T cells enables the recognition of specific tumor antigens, skip antigen presentation. Then, the costimulatory domains in CAR-T cells could activate downstream signaling pathways and trigger antitumor immune responses.[44] On the other hand, the existence of BBB limits the delivery of most cancer therapeutics to the brain parenchyma.[28] However, the pathologic condition of GBM can disrupt the integrity of the BBB to some extent.[45] Moreover, the discovery of lymphatic vessels in the brain and the overturned understanding of brain immunity revealed that T cells could penetrate the BBB and infiltrate the brain in a diffuse manner.[31−33,41] Considerable CAR-T cell infiltration into the glioma site and decreased expression of target antigen were observed in phase I clinical trials of CAR-T cells (NCT02209376, NCT03170141), indicating that CAR-T cells could cross the BBB and target GBM.[9,34] However, despite demonstrating a suitable safety profile and promising antitumor activity, these CAR-T cells failed to achieve the expected therapeutic outcome.[9] Moreover, numerous preclinical studies have shown that although GBM-targeting CAR-T cells exhibited some therapeutic effects, they did not eradicate the tumor completely and therefore could not be effective in the long term.[7,10,46,47] To overcome this limitation of conventional CAR-T cells and improve their therapeutic efficacy against GBM, researchers have attempted to combine them with other drugs. One promising direction is the application of drugs to directly enhance the antitumor activity or proliferative capacity of T cells.[48,49] For example, CAR-T cells combined with IL-12 achieved a durable antitumor response, mainly due to the fact that this cytokine promoted CAR-T cell proliferation.[48] Another effective combination strategy is to apply drugs or therapies that reprogram the immunosuppressive TME such as immune checkpoint inhibitors and oncolytic virotherapy.[50,51] Evidence from preclinical GBM models has demonstrated that combining CAR-T cells with a PD-1-blocking antibody exerted more potent and long-lasting therapeutic effects than CAR-T cell monotherapy.[52]

Although the above combination strategies have improved the efficacy of CAR-T cells against GBM, some limitations remain to be overcome. For instance, in the above-mentioned combination therapies, the CAR-T cells and drugs are administered separately, which leads to their uneven distribution in the body and inconsistent pharmacokinetic behaviors. As a result, the drug and the CAR-T cells exhibit different retention rates at the tumor site and fail to achieve the desired synergistic effect. Moreover, most drugs have more than one corresponding receptor, which can cause off-target toxicity when administered intravenously.[53,54] Thus, techniques that integrate drugs into CAR-T cells, for instance, by genetically engineering T cells to secrete cytokines/chemokines (e.g., IL-12, CCR2, and CCR4)[55−57] or conjugating them to nano drugs (e.g., encapsulated in liposomes),[58−60] are being developed. Herein, we established a cell−drug integrated technology to integrate nanodrug (drug-containing liposomes) onto the surface of CAR-T cells. Briefly, an azide-bearing lipid was hydrophobically anchored to the CAR-T cell membrane, while a DBCO-bearing lipid was used during liposome preparation. Subsequently, liposomes were conjugated to the surface of CAR-T cells through a click reaction between the azide and the DBCO. The ability of the resulting integrated CAR-T cells to transport the nanodrug across the BBB to the glioma site enabled these different therapeutic strategies to act in concert and eradicate the tumor. This combination strategy not only reduces the toxicity of the nanodrug but also improves the therapeutic efficacy of the CAR-T cells.

Multiple barriers impede the therapeutic efficacy of CAR-T cells in GBM. The complex microenvironment of neoplastic and nonneoplastic cells contributes to the formation and progression of the tumor, as well as its response to therapy.[61] In the TME, the majority of nonneoplastic cells are TAMs, which consist of peripheral macrophages recruiting to the tumor site or brain-resident microglia. TAMs contribute to the immunosuppressive TME and support neoplastic cell expansion and invasion.[62] Glioma cells can produce factors to recruit TAMs into the glioma TME. These TAMs then release a variety of growth factors and cytokines in response to the factors produced by glioma cells to promote tumor proliferation, survival, and invasion. Through such iterative interactions, an immunosuppressive TME is established.[14,63] Thus, therapeutically targeting TAMs to remodel the immunosuppressive GBM microenvironment could unleash the full potential of antitumor therapies.

As a CSF-1Ri, PLX can re-educate M2-like TAMs to assume the antitumor M1-like phenotype.[20,64] Thus, in this study, we used PLX as a model drug to generate PLX-Lip. Moreover, to ensure that PLX effectively targeted TAMs, a hydroxide-responsive moiety (AZO) was preintroduced into azide-

https://doi.org/10.1021/acsnano.4c00050
ACS Nano XXXX, XXX, XXX−XXX

bearing lipid. The resulting PLX-Lip cells were then integrated into the surface membrane of CAR-T cells to generate PLX-Lip/AZO-T cells using the cell−drug integrated technology. We showed that the PLX-Lip/AZO-T cells successfully crossed the BBB to reach the glioma site. Exposure to the hypoxic GBM microenvironment caused the PLX-Lip/AZO-T cells to release PLX-Lip, which were then engulfed by TAMs. Assimilation of PLX by the TAMs induced their re-education from the protumorigenic M2-like to the antitumorigenic M1-like phenotype, alleviating immunosuppression, and ultimately enhancing the therapeutic efficacy of the CAR-T cells. The controlled spatiotemporal distribution of drugs conjugated to the surface of CAR-T cells diversifies the spectrum of liposomal drugs that can be used in GBM treatment. Drugs encapsulated in liposomes can target various types of cells in the TME, thus enriching the choice of antitumor therapeutic strategies. However, we acknowledge that our integrated CAR-T cells did not respond sufficiently rapidly to the hypoxic environment, which delayed the release of PLX-Lip and subsequently reduced the efficacy of PLX at the tumor site. Thus, we aim to develop more sensitive TME-responsive strategies (e.g., by using a reversible click reaction with faster responsive bond scission)[65,66] for constructing integrated CAR-T cells in the future.

In summary, we have developed a cell−drug integrated technology and used it to conjugate PLX-Lip to the surface of CAR-T cells as a GBM-targeting combination therapy. These integrated CAR-T cells actively transmigrated across the BBB, thereby dramatically improving the accumulation of PLX-Lip at the glioma site. Moreover, the PLX-Lip cells were released in the hypoxic microenvironment of GBM and effectively taken up by TAMs. The PLX-mediated re-education of TAMs to an M1-like phenotype boosted the antitumor activity of CAR-T cells, which ultimately eradicated the glioma while exhibiting a favorable safety profile. In conclusion, our study introduces a tool for boosting the antitumor efficacy of CAR-T cells, which we envisage will have valuable clinical implications for the treatment of GBM and other solid tumors.

MATERIALS AND METHODS

Human peripheral blood mononuclear cells (hPBMCs) were obtained from the peripheral blood of healthy donors following approval from the Ethics Committee of Nanjing Jingdu Hospital. All the donors had been informed before the experiments. All animal-related experiments were performed in full compliance with animal protocols approved by the China Pharmaceutical University Institutional Animal Care and Use Committee.

Preparation and Characterization of PLX-Lip/AZO-T Cells. *Construction of PLX-Lip/AZO-T Cells.* The chimeric antigen receptor GD2 CAR is composed of extracellular domains of GD2 scFv, extracellular and transmembrane domains of human CD8α, intracellular domains of CD28, 41-BB, and CD3ζ, which was constructed, and packaged the lentivirus by GeneChem Biotechnology Company (Shanghai, China). Naive human $CD3^+$T cells were stimulated with ImmunoCult Human CD3/CD28 T Cell Activator (Stemcell, 25 μL/mL) and cultured in ImmunoCult XF T cell Expansion Medium containing IL-2 at 37 °C and 5% CO_2 for 1 day. Then, the activated T cells were transfected with CAR-expressing lentivirus by a spinoculation method as previously reported. On day 10, the cells were collected and stained with Hoechst 33342 and fixed with 4% PFA for confocal imaging (ZEISS LSM 880 confocal microscope) to investigate the expression of CAR.

PLX-Lip/AZO-T cells were obtained by incubating CAR-T cells sequentially with DSPE-PEG2K-AZO-N_3 and PLX-Lip. Briefly, CAR-T cells (1×10^6 cells/mL) were resuspended in ImmunoCult XF T cell medium. Then, CAR-T cells were incubated with DSPE-PEG2K-AZO-N_3 (18 μM) at 37 °C for 10 min. After washing with ice-cold PBS, cells were incubated with PLX-Lip (PLX:100 μg/mL) at 37 °C for 45 min. After washing with ice-cold PBS, the CAR-T cells surface-anchored PLX-Lip were collected and resuspended in ImmunoCult XF T-cell medium or saline for in vitro or in vivo studies. The concentration of PLX in PLX-Lip/AZO-T cells was determined by HPLC (Shimadzu, HPLC-LC-2010A HT).

Characterization of PLX-Lip/AZO-T Cells. SPC (120 mg), Chol (10 mg), PLX (3 mg), SA_2-DBCO (15 mg), and DHPE-Rhodamine (25 μL, 5 mg/mL) were dissolved in 5 mL of mixture solution, and the Rhodamine B-labeled PLX-Lip were obtained by the same method as for PLX-Lip. Moreover, SPC (120 mg), Chol (10 mg), PLX (3 mg), and DHPE-Rhodamine (25 μL, 5 mg/mL) were dissolved in 5 mL of mixture solution, and the Rhodamine B-labeled PLX-Lip cells without click groups on the surface were obtained by the same method as that used for the preparation of PLX-Lip.

For the preparation of CAR-T cells anchored with fluorescent liposomes, CAR-T cells were incubated with DSPE-PEG2K-AZO-N_3 (18 μM) at 37 °C for 10 min. Then, Rhodamine B-labeled liposomes, with or without click groups on the surface, were incubated with cells at 37 °C for 45 min. After washing with ice-cold PBS, cells were stained with Hoechst 33342, fixed with 4% paraformaldehyde (PFA), and used immediately for confocal imaging (ZEISS LSM 880 confocal microscope) and flow cytometry analysis (Thermo Fisher Scientific). The T cells or CAR-T cells were stained with Hoechst 33342 and fixed with 4% PFA as control.

To calculate the number of PLX-Lip conjugated on the surface of CAR-T cells, CAR-T cells (1×10^6) were first incubated with DSPE-PEG2K-AZO-N_3, and then the cells were incubated with the PLX-Lip solution (1 mL), with or without click groups (DBCO) on the surface. The concentration of PLX-Lip in the solution was assessed with NTA (Zetaview QUATT, Particle Metrix). The liposomes number backpacked on the surface of per CAR-T cell was calculated as follows: $(N_{\text{before PLX-Lip with click groups}} - N_{\text{after PLX-Lip with click groups}})/10^6$ or $(N_{\text{before PLX-Lip without click groups}} - N_{\text{after PLX-Lip without click groups}})/10^6$, where $N_{\text{before PLX-Lip with click groups}}$ and $N_{\text{before PLX-Lip without click groups}}$ were counted numbers of liposomes in the solution before incubation with CAR-T cells, while $N_{\text{after PLX-Lip with click groups}}$ and $N_{\text{after PLX-Lip without click groups}}$ were counted numbers of liposomes in the supernatant after incubation with CAR-T cells.

To further confirm PLX-Lip anchoring on the surface of CAR-T cells, we prepared and collected PLX-Lip/AZO-T cells, after which the cells were fixed overnight using 2.5% glutaraldehyde aqueous solution. After washing three times with PBS, the samples were sectioned and imaged by a Biology transmission electron microscope (Hitachi, HT7800), and the CAR-T cells were fixed and sectioned as control.

Cell Viability, Proliferation, Activation, Cytokine Secretion, and Cell Membrane Fluidity of PLX-Lip/AZO-T Cells. For cell viability, PLX-Lip/AZO-T cells were incubated in ImmunoCult XF T cell medium containing IL-2 and ImmunoCult Human CD3/CD28 T Cell Activator. Cells were collected at 0, 3, 6, 9, and 12 days, respectively. The Annexin V PE-7AAD apoptosis kit (Yeason) was used according to the manufacturer's instructions, and the cell survival was measured by flow cytometry. CAR-T cells were stained with Annexin V PE-7AAD apoptosis kit as control.

For proliferation capacity, CellTrace Far Red cell proliferation assay and tracking kit (Beyotime Biotechnology) were applied according to the manufacturer's instructions. PLX-Lip/AZO-T cells were stained with CellTrace Far Red. After continued incubation in ImmunoCult XF T cell medium containing IL-2 and anti-CD3/CD28, the cells were collected at 0, 3, 6, 9, and 12 days, respectively, and used immediately for flow cytometry analysis. CAR-T cells were stained with CellTrace Far Red as a control.

For activation, PLX-Lip/AZO-T cells were stimulated with anti-CD3/CD28, after 24 h stimulation, the cells were collected and stained with PerCP/Cy5.5 antihuman CD69 antibody (0.5 μg/mL, BioLegend), and expression of the early T cells activation marker

https://doi.org/10.1021/acsnano.4c00050
ACS Nano XXXX, XXX, XXX−XXX

CD69 was quantified by flow cytometry. CAR-T cells were stained with PerCP/Cy5.5 antihuman CD69 antibody as control.

For cytokine secretion, PLX-Lip/AZO-T cells were collected at 0, 3, 6, 9, and 12 days, respectively. Then, the cells were incubated in ImmunoCult XF T cell medium containing phorbol-12-myristate-13-acetate (PMA, 100 ng/mL), ionomycin (2 μM), and the protein transport inhibitor Brefeldin A (BFA, 10 μg/mL). After incubation for 4 h, the cells were collected and washed twice with ice-cold PBS. Then, the cells were fixed with 4% PFA, and incubated with 0.1% Triton X-100 solution for 10 min, washed with PBS, and blocked with nonspecific binding protein for 30 min at r.t with 2% BSA. PE/Cy7 antihuman GzmB antibody (0.8 μg/mL, Biolegend), PerCP antihuman IFN-γ antibody (0.8 μg/mL, Biolegend), PE antihuman TNF-α antibody (0.8 μg/mL, Biolegend) and APC antihuman IL-2 antibody (0.8 μg/mL, Biolegend) was added to cells and the cells were incubated for 30 min. The cytokine secretion of PLX-Lip/AZO-T cells was investigated by flow cytometry. CAR-T cells were treated as a control.

For cell membrane fluidity, PLX-Lip/AZO-T cells were resuspended with ImmunoCult XF T cell medium containing 5 μM fluorescent lipid reagents and 0.08% PluronicF127, and cultured at 25 °C for 1 h in darkness. Then, cells were washed twice and the fluorescence of cells at 400 and 470 nm was determined by a microplate reader (BioTek Instruments, Inc., Synergy H1, USA) with an excitation wavelength of 350 nm. Subtract the blank(s) from each sample to calculate the normalized excimer-to-monomer fluorescence ratio (Ie/Im) from the average of repeated readings. Moreover, cells were cultured at 25 °C for 1 h without fluorescent lipid reagents as control.

Stability of Liposomes or Drug on the Surface of PLX-Lip/AZO-T Cells. To evaluate the stability of PLX-Lip on the surface of T cells, fluorescently labeled PLX-Lip/AZO-T cells were prepared using DSPE-PEG2K-AZO-N_3 and fluorescent liposomes. After being incubated in the medium containing IL-2 (10 ng/mL), ImmunoCult Human CD3/CD28 T Cell Activator (25 μL/mL) with 37 °C, 5% CO_2 for different times (0, 3, 6, 12, 24, 48 h), the cells were collected and washed with ice-cold PBS. Then, the cells were stained with Hoechst 33342, fixed with 4% PFA, and used immediately for confocal imaging.

To further investigate the stability of the drug on the surface of cells, 1×10^6 PLX-Lip/AZO-T cells were collected and decomposed with SDS, then added CH_3CN for protein precipitation and drug extraction. Vortex for 3 min and centrifuged (12,000 rpm, 10 min) to get supernatant for HPLC analysis.

To evaluate the stability of PLX-Lip on the surface of T cells in the serum-containing medium, PLX-Lip/AZO-T cells were prepared using DSPE-PEG2K-AZO-N_3 and fluorescent liposomes and resuspended in the medium containing 50% fetal bovine serum (FBS, Gibco) for 0, 1, 3, 6, 12, 24, and 48 h. Then, 1×10^6 PLX-Lip/AZO-T cells were collected and decomposed with SDS, added CH_3CN for protein precipitation and drug extraction. The cells were vortexed for 3 min and centrifuged (12,000 rpm, 10 min) to get supernatant for HPLC analysis.

Moreover, the loading drug stability of PLX-Lip/AZO-T cells was investigated under blood flow shear force. Briefly, PLX-Lip/AZO-T cells were collected and resuspended with PBS (2×10^6 cells/mL), and then the cells were added to a rectangular area (0.5 cm × 1 cm) in the center of a 20 nm dish, which has been plated 0.01% polylysine (PLL) at 4 °C overnight. Then, the cells were left to adsorb on the bottom of the dish for 10 min. The card slot is fixed in the rectangular area. One end of the card slot is connected to the liquid flow pump, which injects PBS, and the other end is connected to a plastic hose to collect the outflow liquid. The flow rate was controlled so that the shear force was 2 dyn/cm^2 (simulating the shear force at the inflammatory microvessel) and 6 dyn/cm^2 (simulating the shear force at the arterial vessel). The cells were rinsed at different flow rates for 3 min, then the rinsing solution was collected, lyophilized, and dissolved with CH_3CN, and the amount of PLX shed under the impact of blood shear force was determined by HPLC analysis.

The stability of drug loading on the cells after transvascular migration also was measured. Human umbilical vein endothelial cells (HUVECs) were applied to construct a trans-well model as previously reported. After the trans-well model was constructed successfully, the HUVEC monolayers were stimulated with 25 ng/mL TNF-α for 4 h. Then, PLX-Lip/AZO-T cells (1×10^6) were added to the upper chamber, and the glioma condition medium (the culture supernatant of LN-229 cells, GCM), which was the supernatant incubation of the LN-229 cells with DMEM complete medium, was added into the lower chamber to induce the migration. After 12 h of incubation, cells and supernatant in the lower chamber were collected. Then, the number of T cells in the lower chamber was counted by hemocytometer (CountStar BioMed), and the amounts of PLX in the supernatant or cells were determined using HPLC.

Tumor-Targeting Ability of PLX-Lip/AZO-T Cells. *Tumor-Targeting Ability of PLX-Lip/AZO-T Cells In Vitro.* To investigate the tumor-targeting ability of PLX-Lip/AZO-T cells, the chemotaxis and migration of PLX-Lip/AZO-T cells toward tumor cells were measured in vitro. For chemotactic ability, PLX-Lip/AZO-T cells (1×10^6) were placed in the upper chamber of the trans-well dish, and T cell medium containing 0, 50, and 100% of GCM was added to the lower chamber. After 12 h of incubation, the cells in the lower chamber were collected and counted using a hemocytometer, and the chemotactic index was calculated according to the following formula. The chemotactic index = $(N_{\text{PLX-Lip/AZO-T cell}} - N_{\text{control}})/1 \times 10^6$, where $N_{\text{PLX-Lip/AZO-T cell}}$ and N_{control} were counted the number of cells in the lower chamber after incubating with PLX-Lip/AZO-T cells in the presence of GCM and the unmodified CAR-T cells in the absence of GCM, respectively.

For the migration ability of PLX-Lip/AZO-T cells, HUVEC cells were applied to construct a trans-well model and stimulated by TNF-α (25 ng/mL) for 4 h. Then, the PLX-Lip/AZO-T cells (1×10^6) or CAR-T cells (1×10^6) were added to the upper chamber, respectively, and the GCM was added to the lower chamber. After 12 h of incubation, cells in the upper chamber and lower chamber were collected. Cell counts were performed to measure the ability of PLX-Lip/AZO-T cells to converge across blood vessels toward tumor cells.

Moreover, the drug on the surface of CAR-T cells toward tumors also were investigated. HUVEC cells were applied to construct a trans-well model and stimulated by TNF-α (25 ng/mL) for 4 h. Then, PLX-Lip/AZO-T cells (1×10^6), PLX-Lip (4.9 μg/mL), or PLX (4.9 μg/mL) were added to the upper chamber, respectively, and the GCM was added into the lower chamber. After 12 h of incubation, the cells and supernatant in the lower chamber were collected, and the amounts of PLX in the lower chamber were measured by HPLC.

Tumor-Targeting Ability of PLX-Lip/AZO-T Cells In Vivo. Human luciferase-expressing glioblastoma cells (LN-229-Luci cells, 5×10^5 cells/5 μL) were injected into the right frontal lobe of BALB/c nude mice using a microsyringe to generate the intracranial glioma model. To further demonstrate the in vivo tumor targeting and biodistribution of PLX-Lip/AZO-T cells, CAR-T cells were labeled with DID, and PLX-Lip were labeled with DIR for convenient imaging. Then, the glioma mice were randomly divided into three groups and received DIR-labeled PLX-Lip (2 mg/kg for PLX), DID-labeled CAR-T cells (2×10^7), and PLX-Lip/AZO-T cells (2×10^7, 2 mg/kg for PLX, cells were labeled with DID and PLX-Lip were labeled with DIR) by intravenous injection on day 7 after tumor inoculation. At 6, 12, 24, 48, and 72 h postinjection, the fluorescence intensity of liposomes and cells at intracranially glioma sites was measured by IVIS Spectrum Imaging System (PerkinElmer). Then, the mice were sacrificed after the blood collection, and the tissues including the tumor, heart, liver, spleen, lung, and kidney were harvested for the IVIS Spectrum Imaging System (PerkinElmer). Living Image software (PerkinElmer) was used to acquire and quantify the bioluminescence imaging data sets.

The blood was centrifugated and the cells were lysed of red blood cells and isolated by 40 to 70% Percoll (GE) gradient centrifugation to obtain lymphocytes. The lymphocytes were stained with APC-Cy7 antihuman CD3 antibody (0.5 μg/mL, Biolegend) and were

https://doi.org/10.1021/acsnano.4c00050
ACS Nano XXXX, XXX, XXX−XXX

measured by flow cytometry to determine the CAR-T quantity in blood. Moreover, the blood was centrifugated and the serum was collected. Then, the serum was added to a protein precipitator (acetonitrile: methanol = 2:1), followed by a vortex for 5 min and centrifugation at 12,000 rpm for 10 min. The supernatant was analyzed by HPLC to determine the concentration of PLX in blood. The tumors were weighed and digested by collagenase IV (Sangon Biotech) to obtain a single-cell suspension. Then, the lymphocyte was isolated by 40 to 70% Percoll (GE) gradient centrifugation and analyzed by flow cytometry to determine the CAR-T quantity in tumors. For analysis of the PLX amount in tumors, the tumors were weighted and homogenized in saline, the homogenate was diluted with 10% $NaHCO_3$ aqueous solution and mixed with acetonitrile, followed by vortex for 5 min and centrifugation at 12,000 rpm for 10 min. Then, the supernatant was quantified by HPLC to determine the concentration of PLX in tumors.

Hypoxia-Responsive Release of PLX-Lip from PLX-Lip/AZO-T Cells In Vitro and In Vivo. To investigate the shedding of PLX-Lip on the surface of PLX-Lip/AZO-T cells under hypoxic conditions, PLX-Lip/T cells were first prepared as a control, which was the PLX-Lip anchored on the surface of CAR-T cells, and the PLX-Lip do not detach from the CAR-T cells under hypoxic conditions. Briefly, CAR-T cells were first coincubated with DSPE-PEG2K−N_3, which does not contain azobenzene groups. After that, the cells were coincubated with Rhodamine B-labeled PLX-Lip in the same method as PLX-Lip/AZO-T cells to obtain Rhodamine B-labeled PLX-Lip/T cells.

Hypoxia-Responsive Release of PLX-Lip from PLX-Lip/AZO-T Cells In Vitro. Rhodamine B-labeled PLX-Lip/AZO-T cells or PLX-Lip/T cells were cultured in ImmunoCult XF T cell medium containing 2 mg/mL liver microsomes and 1 mM NADPH. After incubation in the anaerobic system (94 N_2, 5 CO_2, and 1% O_2; SANYO, MCO-5M) simulating the hypoxic microenvironment of gliomas for different times (0, 1, 3, 6, and 12 h), cells were collected and the liposomes remaining on the surface of cells was investigated by confocal imaging and flow cytometry analysis. The amount of liposomes remained on the CAR-T cells under the anaerobic system was measured using NTA and the number of liposomes remaining per CAR-T cell was calculated as follows: $[(N_{\text{before PLX-Lip}} - N_{\text{after PLX-Lip}}) - N_{\text{after incubation}}]/10^6$, where $N_{\text{before PLX-Lip}}$ and $N_{\text{after PLX-Lip}}$ were counted numbers of PLX-Lip in the solution before and after incubation with CAR-T cells to prepare PLX-Lip/AZO-T cells, while $N_{\text{after incubation}}$ was counted numbers of PLX-Lip in the supernatant after PLX-Lip/AZO-T cells incubation in an anaerobic system. PLX-Lip/T cells were used as the control. Moreover, the drug amount of PLX was released from PLX-Lip/AZO-T cells or PLX-Lip/T cells under the anaerobic system at different times also were investigated using HPLC.

Uptake of PLX-Lip by TAMs and Glioma Cells. Equal amounts of LN-229 cells and TAMs were placed in the same well of a 24-well plate, then RhoB-labeled PLX-Lip released from PLX-Lip/AZO-T cells was added and then coincubated for 2 h. Cells were collected and stained with antimouse F4/80 antibody (Biolegend, 1 μg/mL). Flow cytometry was used to investigate the ratio of $F4/80^+RhoB^+$ (liposomes taken up by TAMs) to $F4/80^-RhoB^+$ (liposomes taken up by LN-229 cells).

Determination of Antitumor Effect to Glioma Cells of PLX-Lip Released from PLX-Lip/AZO-T Cells. Equal amounts of LN-229 cells were placed in the same well of a 12-well plate for 12 h, then blank medium, PLX-Lip solution, PLX-Lip/AZO-T cells (the culture supernatant of 5×10^6 cells treated with medium containing liver microsomes and NADPH, which was placed in the anaerobic system using tri-gas incubator for 12 h, 60 nM for PLX), was added, respectively. The above cells were coincubated for 24 h and harvested to stain with antihuman Ki-67 antibody (Biolegend, 1 μg/mL). Use flow cytometry to detect the expression levels of Ki-67 in LN-229 cells.

Intratumorally Responsive Release of PLX-Lip from PLX-Lip/AZO-T Cells. PLX-Lip/AZO-T cells (2×10^7) or PLX-Lip/T cells (2×10^7) were prepared with DIR-labeled PLX-Lip and injected intravenously into glioma mice (n = 3 mice/group). The accumulation of cells in the tumor peaked at 48 h after injection. Taking this time point as the starting point, the tumor tissues isolated at 0, 2, 6, and 12 h were soaked in 30% sucrose solution for 24 h for dehydration, the surface water of the tissues was drained, and the tissues were cut into slices with a thickness of 8 μm using a cryotome and stored at −20 °C. The frozen slices were removed from the −20 °C refrigerator and dried at rt for 15 min, and soaked in PBS for 10 min to remove the embedding agent. The tissue to be stained was circled with an immunohistochemical pen, stained with Hoechst 33342 and Cy3 antimouse F4/80 antibody, washed with PBS (6 × 6 min), sealed with 90% glycerin, and photographed by NanoZoomer S60 (Hamamatsu Photonics Co., Ltd., C13210-01, Japan). Meanwhile, the tumor tissues isolated at 0 and 12 h were digested with collagenase IV to obtain single-cell suspension. Then, lymphocytes were isolated by 40 to 70% Percoll (GE) gradient centrifugation and stained by Cy3 antimouse F4/80 antibody. After washing twice with ice-cold PBS, cells were analyzed by flow cytometry to further determine the distribution of liposomes in CAR-T cells or TAMs.

Mechanism Research of PLX-Lip/AZO-T Cells In Vitro and In Vivo. *Mechanism Research of PLX-Lip/AZO-T Cells In Vitro.* To study the mechanism of PLX-Lip/AZO-T cells in vitro, microglia in the brain and the macrophage in bone marrow were first isolated and polarized into M2 phenotype to simulate the TAMs. For microglia, C57BL/6J suckling mice, which were born in 24−48 h, were disinfected. Then, the brain tissue was separated and digested with 0.25% tryptase at 37 °C for 6 min, and DMEM medium containing 10% FBS was added to terminate digestion. The cells were centrifuged (1500 rpm, 10 min) and the blood filament at the bottom of the tube was removed. Afterward, the cells were passed through a 0.7 μm cell sieve to remove incompletely digested tissue. Then, the cells were cultured in T75 culture bottles, which were coated with 0.1% PLL in advance. After incubation of 48 h, the culture bottle was slightly shaken for 1 min and the fluid was changed to remove the cell fragments. After the cells were continuously incubated for 96 h, the cell fragments were removed again, and then microglia were collected every 4−6 days (the medium was sucked after rapid shock and centrifuged at 1500 rpm for 10 min). The resulting cells were inoculated into 24-well plates at a density of 1×10^5 per well (the plates were coated with PLL in advance). For M2 polarization, microglia were stimulated with a DMEM medium containing 10% FBS and 20 ng/mL IL-4 or GCM for 24 h. For macrophages, bone marrow was flushed from femur and tibia bones of 6−10 weeks BALB/c mice by DMEM medium. After centrifugation at 200 g for 3 min and lysis with erythrocyte lysis buffer for 3 min, the unicellular suspension (1×10^6 cells) was cultured for 7 days in 10 mL of DMEM medium supplemented with 10% FBS and 10 ng/mL macrophage-stimulating factor (M-CSF) to obtain adherent macrophages. To polarize the macrophages to M2-like phenotype, macrophages were stimulated with a DMEM medium containing 10% FBS and 20 ng/mL IL-4 for 24 h.

To evaluate the effect of PLX-Lip/AZO-T cells to reverse the phenotype of TAMs in vitro, M2-like microglia or M2-like macrophages were cultured in 12-well plates (5×10^5 cells/well). Then, GCM, PLX (60 nM), PLX-Lip (60 nM for PLX), CAR-T cells (The culture supernatant of 5×10^6 cells for 12 h), or PLX-Lip/AZO-T cells (The culture supernatant of 5×10^6 cells treated with medium containing liver microsomes and NADPH, which was placed in the anaerobic system using tri-gas incubator for 12 h, 60 nM for PLX) was added, respectively. After incubation for 24 h, the cells were collected and stained with PE antimouse CD80 antibody and APC antimouse CD206 antibody and were measured by flow cytometry. Moreover, the M2-like microglia were treated with different groups as described earlier and the phenotype-reversed cells were collected. The total RNA of cells was isolated using the TransZol reagent (Transgene) following the manufacturer's protocol. Then, the total RNA (1 μg) was reverse-transcribed to cDNA using a first-strand cDNA synthesis kit (TaKaRa). Real-time PCR was performed using the StepOnePlus real-time PCR system (Applied Biosystems) and AceQ qPCR SYBR Green Master Mix (Vazyme). The quantification of mRNA expression containing *Il1b*, *Ifna*, *Tgfb*, and *Il10* was performed, and the

https://doi.org/10.1021/acsnano.4c00050
ACS Nano XXXX, XXX, XXX−XXX

amplification procedure parameters were set as follows: 95 °C, heating for 10 s, 60 °C, heating for 20 s, and 45 cycles were repeated. After the cyclic amplification was completed, the Ct value (Ct value: the number of cycles when the fluorescence signal of the sample reached the set threshold) was obtained by using β-actin as the internal parameter. The expression efficiency of the target gene (%) = $2^{-\Delta\Delta T} \times 100\%$; ΔT = Ct (target gene) − Ct (β-actin), $\Delta\Delta T = \Delta T - \Delta T_{control}$. The primers used in this experiment are shown in Table 1.

Table 1. Primers of Inflammatory Factor

name	primers
Tnfa	forward: TAGCCCACGTCGTAGCAAAC
	reverse: ACCCTGAGCCATAATCCCCT
Il1b	forward: TGCCACCTTTTGACAGTGATG
	reverse: TTCTTGTGACCCTGAGCGAC
Il10	forward: GCTCCAAGACCAAGGTGTCT
	reverse: AGGACACCATAGCAAAGGGC
Tgfb	forward: ACTGGAGTTGTACGGCAGTG
	reverse: GGGGCTGATCCCGTTGATTT
β-actin	forward: GGCTGTATTCCCCTCCATCG
	reverse: CCAGTTGGTAACAATGCCATGT

To evaluate the phagocytic activity of phenotypically reversed TAMs, M2-like TAMs were treated with different groups as described earlier. After treated for 24 h, the phenotype-reversed cells were collected and centrifugated (1000 rpm, 5 min). Then, the supernatant was discarded, and the cells were coincubated with the Hoechst-labeled LN-229 cells for 24 h. Then, the cells were collected, stained with PerCP/Cy5.5 antimouse F4/80 antibody, and investigated the proportion of $F4/80^+$ $Hoechst^+$ cells in $F4/80^+$ cells using flow cytometry. Untreated microglia were used as a control. Meanwhile, the cells were also collected to detect the expression level of ROS according to the manufacturer's protocol.

To further explore the effects of phenotype-reversed TAMs on the apoptosis and proliferation of glioma cells. M2-like TAMs were treated with different groups as described previously. Then, M2-like TAMs were coincubated with LN-229-luci cells for 24 h. 100 μL D-Fluorescein potassium salt was added into the medium, and bioluminescence was detected by a microplate reader to evaluate the apoptosis of LN-229-Luci cells. Besides, the LN-229-luci cells also were collected and stained with Ki-67 (Biolegend, 1 μg/mL).

To further evaluate the effect of phenotypically reversed TAM on the viability and cytokine secretion of CAR-T cells. M2-like microglia were treated with different groups as described previously. After 24 h incubation, the phenotypically reversed cells were collected and centrifuged (1000 rpm, 5 min). Then, the supernatant was discarded, and the cells were incubated with CAR-T cells (5×10^5) for 24 h. Cells were collected, and some cells were treated with the Annexin V-PE/7AAD apoptosis kit (Yeason) according to the manufacturer's protocol. Moreover, other cells were fixed with 4% PFA, and incubated with 0.1% Triton for 10 min, washed with PBS, and blocked with nonspecific binding protein for 30 min at r.t. with 2% BSA. PE antihuman GzmB antibody, APC antihuman IFNγ antibody, and APC/Cy7 antihuman TNF-α antibody were added to the cells and incubated for 30 min. Besides, cell culture supernatants were also collected to detect the release of TNF-α, IFNγ, and GzmB by ELISA kit according to the manufacturer's protocol. The viability and cytokine secretion of CAR-T cells were investigated by flow cytometry and ELISA. Untreated microglia were used as a control.

Mechanism Research of PLX-Lip/AZO-T Cells In Vivo. To investigate the ability of PLX-Lip/AZO-T cells to reverse the phenotype of TAMs and the effects of phenotypically reversed TAMs on the adoptively transfer CAR-T cells in vivo, glioma mice were randomly divided into 5 groups with 3 mice in each group, and were injected intravenously with saline, PLX (5 mg/kg), PLX-Lip (5 mg/kg for PLX), CAR-T cells (2×10^7), or PLX-Lip/AZO-T cells (2×10^7, 5 mg/kg for PLX) on days 7 and 12 after tumor inoculation, respectively. On day 14, mice were sacrificed, and tumors were harvested. After tumors were digested and gradient centrifuged, leukocytes were isolated and stained with APC/Cy7 antimouse CD45, APC antimouse F4/80 antibody, PE/Cy7 antimouse CD80 antibody, and AF488 antimouse CD206 antibody. After washing twice with ice-cold PBS, the cells were detected by flow cytometry, and the polarization phenotype of TAM was investigated. In addition, some leukocytes isolated from the tumors of CAR-T cells and PLX-Lip/AZO-T cells groups were stained with PE/Cy7 antihuman GzmB antibody, PerCP antihuman IFN-γ antibody, PE antihuman TNF-α antibody, and APC antihuman IL-2 antibody and measured by flow cytometry.

Pharmacodynamics and Safety of PLX-Lip/AZO-T Cells. *Pharmacodynamics of PLX-Lip/AZO-T Cells In Vivo.* Glioma mice were randomly divided into 7 groups with 8 mice in each group and were injected intravenously with saline, PLX (5 mg/kg), PLX-Lip (5 mg/kg for PLX), CAR-T cells (2×10^7), PLX+CAR-T cells (2×10^7 CAR-T + 5 mg/kg PLX), PLX-Lip/T cells (2×10^7, 5 mg/kg for PLX), or PLX-Lip/AZO-T cells (2×10^7, 5 mg/kg for PLX) on days 7 and 12 after tumor inoculation, respectively. From day 6, mice were imaged for bioluminescence every 4 days to monitor the tumor growth, and survival of mice was recorded every day. Euthanasia was performed when the weight of the mice was reduced to 20% of the weight before administration, or the mice died naturally. The above conditions were included in the death data, and the survival curve of the mice was finally obtained according to the statistics of the survival status of the mice.

Safety Profile of PLX-Lip/AZO-T Cells In Vivo. Weight of glioma mice were recorded on days 0, 2, 4, 6, 8, 10, 12, 14, 16, 18, and 20 after tumor implantation. The heart, liver, spleen, lung, and kidney of mice were collected and weighed to calculate the organ index. Moreover, these tissues were dissected, embedded in paraffin, sectioned, and stained with H&E using routine methods as previously reported. Then, the sections were photographed using doltSlide virtual microscopy (Olympus). The blood samples from each group of mice were collected on day 18 after tumor inoculation and centrifuged (12,000 rpm, 10 min). The quantities of ALP, LDH, AST, ALT, BUN, and CRE in the supernatant were, respectively, determined per kit instructions, and IL-6, IL-10, and TNF-α concentrations were analyzed via ELISA kit (Elabscience).

Statistical Analysis. Statistical analyses were performed using GraphPad Prism 8.0. All plots show mean ± SEM. One-way ANOVA test and two-way ANOVA with Tukey's correction were used for comparisons of multiple groups and a student's unpaired *t*-test was used for two-group comparisons under the appropriate conditions. A log-rank (Mantel-Cox) test was used to analyze survival differences. Statistical significance was set at $^*P < 0.05$, $^{**}P < 0.01$, $^{***}P < 0.001$, and $^{****}P < 0.0001$, ns: no significant difference.

ASSOCIATED CONTENT

Supporting Information

The Supporting Information is available free of charge at https://pubs.acs.org/doi/10.1021/acsnano.4c00050.

Materials and methods including the detailed methods of the synthesis of DSPE-PEG2k-AZO-N_3 and SA_2-DBCO, preparations and characterization of the liposomes, cell culture, and isolation of the primary cells; synthesis of DSPE-PEG2K-AZO-N_3 and SA_2-DBCO; ^{1}H NMR spectra of DSPE-PEG2K-AZO-N_3 and SA_2-DBCO; UV absorbance of azobenzene bone in DSPE-PEG2K-AZO-N_3 at different time under hypoxic conditions; Figures S4−S5, characteristics of the PLX-Lip; characteristics of GD2 CAR-T cells; optimal preparation conditions of PLX-Lip/AZO-T cells; characteristics of PLX-Lip/AZO-T cells; drug-loading stability of PLX-Lip/AZO-T cells in serum-containing medium; construction of orthotopic GBM-bearing mice

https://doi.org/10.1021/acsnano.4c00050
ACS Nano XXXX, XXX, XXX−XXX

model; biodistribution of CAR-T cells and PLX-Lip in vivo; characteristics of integrated CAR-T cells not responsive to hypoxia; release of PLX and PLX-Lip from PLX-Lip/AZO-T cells under hypoxic conditions with time; uptake of PLX-Lip released from PLX-Lip/AZO-T cells by TAMs and the direct antitumor effect of PLX-Lip; extraction and induction of M2-like TAMs in vitro; function of PLX-Lip/AZO-T cells in vitro and in vivo; and safety evaluation of PLX-Lip/AZO-T cells in orthotopic GBM-bearing mice (PDF).

AUTHOR INFORMATION

Corresponding Authors

Meixi Hao − *State Key Laboratory of Natural Medicines, Center of Advanced Pharmaceuticals and Biomaterials, China Pharmaceutical University, Nanjing 211198, China; Chongqing Innovation Institute of China Pharmaceutical University, Chongqing 401135, China*; Email: haomeixi@cpu.edu.cn

Can Zhang − *State Key Laboratory of Natural Medicines, Center of Advanced Pharmaceuticals and Biomaterials, China Pharmaceutical University, Nanjing 211198, China; Chongqing Innovation Institute of China Pharmaceutical University, Chongqing 401135, China*; orcid.org/0000-0003-3529-5438; Email: zhangcan@cpu.edu.cn

Authors

Nianci Zhu − *State Key Laboratory of Natural Medicines, Center of Advanced Pharmaceuticals and Biomaterials, China Pharmaceutical University, Nanjing 211198, China; Chongqing Innovation Institute of China Pharmaceutical University, Chongqing 401135, China*

Sijia Chen − *State Key Laboratory of Natural Medicines, Center of Advanced Pharmaceuticals and Biomaterials, China Pharmaceutical University, Nanjing 211198, China; Chongqing Innovation Institute of China Pharmaceutical University, Chongqing 401135, China*

Yu Jin − *State Key Laboratory of Natural Medicines, Center of Advanced Pharmaceuticals and Biomaterials, China Pharmaceutical University, Nanjing 211198, China; Chongqing Innovation Institute of China Pharmaceutical University, Chongqing 401135, China*

Meng Wang − *State Key Laboratory of Natural Medicines, Center of Advanced Pharmaceuticals and Biomaterials, China Pharmaceutical University, Nanjing 211198, China; Chongqing Innovation Institute of China Pharmaceutical University, Chongqing 401135, China*

Luyao Fang − *State Key Laboratory of Natural Medicines, Center of Advanced Pharmaceuticals and Biomaterials, China Pharmaceutical University, Nanjing 211198, China; Chongqing Innovation Institute of China Pharmaceutical University, Chongqing 401135, China*

Lingjing Xue − *State Key Laboratory of Natural Medicines, Center of Advanced Pharmaceuticals and Biomaterials, China Pharmaceutical University, Nanjing 211198, China; Chongqing Innovation Institute of China Pharmaceutical University, Chongqing 401135, China*

Dexiang Hua − *State Key Laboratory of Natural Medicines, Center of Advanced Pharmaceuticals and Biomaterials, China Pharmaceutical University, Nanjing 211198, China; Chongqing Innovation Institute of China Pharmaceutical University, Chongqing 401135, China*

Ziyao Zhang − *State Key Laboratory of Natural Medicines, Center of Advanced Pharmaceuticals and Biomaterials, China Pharmaceutical University, Nanjing 211198, China; Chongqing Innovation Institute of China Pharmaceutical University, Chongqing 401135, China*

Meng Jia − *School of Life Sciences, Nanjing University, Nanjing 210093, China*

Complete contact information is available at: https://pubs.acs.org/10.1021/acsnano.4c00050

Author Contributions

N.Z. designed and conducted most experiments and analyzed the data; S.C. conducted all animal experiments, analyzed the data, and wrote the original manuscript; Y.J. assisted in all experiments; M.W. and L.F. assisted in analyzing the data and wrote the manuscript; L.X. assisted in analyzing the data; D.H., Z.Z., and M.J. assisted in mice experiments; M.H. supervised all experiments and wrote the manuscript; C.Z. conceived the project and supervised all the experiments; N.Z. and S.C. contributed equally to this work.

Notes

The authors declare no competing financial interest.

ACKNOWLEDGMENTS

We thank the Public Platform of the State Key Laboratory of Natural Medicines for assistance with the imaging of pathological sections and Nanjing Jingdu Hospital for assistance with the recruitment of volunteers and peripheral blood collection. Funding: This work was supported by the National Natural Science Foundation of China (82130102 to C.Z., 92159304 to C.Z., 81930099 to C.Z., 81773664 to C.Z., 82373823 to M.H. and 82104102 to M.H.), the Natural Science Foundation of Jiangsu Province (BK20212011 to C.Z., and BK20230104 to M.H.), Technology innovation project of Nucleic acid drug from National Center of Technology Innovation for Biopharmaceuticals (NCTIB2022HS01014 to C.Z.), "Double First-Class" University project (CPU2022QZ05 to C.Z.), Project Program of State Key Laboratory of Natural Medicines (China Pharmaceutical University, SKLNMZZ202310 to C.Z., SKLNMZZ202223 to C.Z.), and the Fundamental Research Funds for the Central Universities of China (China Pharmaceutical University, 2632023TD01 to M.H.).

REFERENCES

(1) Ostrom, Q. T.; Price, M.; Neff, C.; Cioffi, G.; Waite, K. A.; Kruchko, C.; Barnholtz-sloan, J. S. CBTRUS Statistical Report: Primary Brain and Other Central Nervous System Tumors Diagnosed in the United States in 2015−2019. *Neuro Oncol.* **2022**, *24* (Suppl 5), v1−v95.

(2) Tan, A. C.; Ashley, D. M.; López, G. Y.; Malinzak, M.; Friedman, H. S.; Khasraw, M. Management of Glioblastoma: State of the Art and Future Directions. *CA Cancer J. Clin* **2020**, *70* (4), 299−312.

(3) Stupp, R.; Mason, W. P.; Van den bent, M. J.; Weller, M.; Fisher, B.; Taphoorn, M. J. B.; Belanger, K.; Brandes, A. A.; Marosi, C.; Bogdahn, U.; Curschmann, J.; Janzer, R. C.; Ludwin, S. K.; Gorlia, T.; Allgeier, A.; Lacombe, D.; Cairncross, J. G.; Eisenhauer, E.; Mirimanoff, R. O. European Organisation for Research and Treatment of Cancer Brain Tumor and Radiotherapy Groups; National Cancer Institute of Canada Clinical Trials Group. Radiotherapy plus Concomitant and Adjuvant Temozolomide for Glioblastoma. *N Engl J. Med.* **2005**, *352* (10), 987−996.

(4) Lim, M.; Xia, Y.; Bettegowda, C.; Weller, M. Current State of Immunotherapy for Glioblastoma. *Nat. Rev. Clin Oncol* **2018**, *15* (7), 422−442.
(5) Liau, L. M.; Ashkan, K.; Brem, S.; Campian, J. L.; Trusheim, J. E.; Iwamoto, F. M.; Tran, D. D.; Ansstas, G.; Cobbs, C. S.; Heth, J. A.; Salacz, M. E.; D'andre, S.; Aiken, R. D.; Moshel, Y. A.; Nam, J. Y.; Pillainayagam, C. P.; Wagner, S. A.; Walter, K. A.; Chaudhary, R.; Goldlust, S. A.; Lee, I. Y.; Bota, D. A.; Elinzano, H.; Grewal, J.; Lillehei, K.; Mikkelsen, T.; Walbert, T.; Abram, S.; Brenner, A. J.; Ewend, M. G.; Khagi, S.; Lovick, D. S.; Portnow, J.; Kim, L.; Loudon, W. G.; Martinez, N. L.; Thompson, R. C.; Avigan, D. E.; Fink, K. L.; Geoffroy, F. J.; Giglio, P.; Gligich, O.; Krex, D.; Lindhorst, S. M.; Lutzky, J.; Meisel, H.-J.; Nadji-ohl, M.; Sanchin, L.; Sloan, A.; Taylor, L. P.; Wu, J. K.; Dunbar, E. M.; Etame, A. B.; Kesari, S.; Mathieu, D.; Piccioni, D. E.; Baskin, D. S.; Lacroix, M.; May, S.-A.; New, P. Z.; Pluard, T. J.; Toms, S. A.; Tse, V.; Peak, S.; Villano, J. L.; Battiste, J. D.; Mulholland, P. J.; Pearlman, M. L.; Petrecca, K.; Schulder, M.; Prins, R. M.; Boynton, A. L.; Bosch, M. L. Association of Autologous Tumor Lysate-Loaded Dendritic Cell Vaccination With Extension of Survival Among Patients With Newly Diagnosed and Recurrent Glioblastoma: A Phase 3 Prospective Externally Controlled Cohort Trial. *JAMA Oncol* **2023**, *9* (1), 112−121.
(6) Todo, T.; Ito, H.; Ino, Y.; Ohtsu, H.; Ota, Y.; Shibahara, J.; Tanaka, M. Intratumoral Oncolytic Herpes Virus G47Δ for Residual or Recurrent Glioblastoma: A Phase 2 Trial. *Nat. Med.* **2022**, *28* (8), 1630−1639.
(7) Ahmed, N.; Brawley, V.; Hegde, M.; Bielamowicz, K.; Kalra, M.; Landi, D.; Robertson, C.; Gray, T. L.; Diouf, O.; Wakefield, A.; Ghazi, A.; Gerken, C.; Yi, Z.; Ashoori, A.; Wu, M.-F.; Liu, H.; Rooney, C.; Dotti, G.; Gee, A.; Su, J.; Kew, Y.; Baskin, D.; Zhang, Y. J.; New, P.; Grilley, B.; Stojakovic, M.; Hicks, J.; Powell, S. Z.; Brenner, M. K.; Heslop, H. E.; Grossman, R.; Wels, W. S.; Gottschalk, S. HER2-Specific Chimeric Antigen Receptor-Modified Virus-Specific T Cells for Progressive Glioblastoma: A Phase 1 Dose-Escalation Trial. *JAMA Oncol* **2017**, *3* (8), 1094−1101.
(8) Prapa, M.; Chiavelli, C.; Golinelli, G.; Grisendi, G.; Bestagno, M.; Di tinco, R.; Dallora, M.; Neri, G.; Candini, O.; Spano, C.; Petrachi, T.; Bertoni, L.; Carnevale, G.; Pugliese, G.; Depenni, R.; Feletti, A.; Iaccarino, C.; Pavesi, G.; Dominici, M. GD2 CAR T Cells against Human Glioblastoma. *NPJ Precis. Oncol.* **2021**, *5* (1), 93.
(9) O'rourke, D. M.; Nasrallah, M. P.; Desai, A.; Melenhorst, J. J.; Mansfield, K.; Morrissette, J. J. D.; Martinez-lage, M.; Brem, S.; Maloney, E.; Shen, A.; Isaacs, R.; Mohan, S.; Plesa, G.; Lacey, S. F.; Navenot, J.-M.; Zheng, Z.; Levine, B. L.; Okada, H.; June, C. H.; Brogdon, J. L.; Maus, M. V. A Single Dose of Peripherally Infused EGFRvIII-Directed CAR T Cells Mediates Antigen Loss and Induces Adaptive Resistance in Patients with Recurrent Glioblastoma. *Sci. Transl. Med.* **2017**, *9* (399), No. eaaa0984.
(10) Brown, C. E.; Alizadeh, D.; Starr, R.; Weng, L.; Wagner, J. R.; Naranjo, A.; Ostberg, J. R.; Blanchard, M. S.; Kilpatrick, J.; Simpson, J.; Kurien, A.; Priceman, S. J.; Wang, X.; Harshbarger, T. L.; D'apuzzo, M.; Ressler, J. A.; Jensen, M. C.; Barish, M. E.; Chen, M.; Portnow, J.; Forman, S. J.; Badie, B. Regression of Glioblastoma after Chimeric Antigen Receptor T-Cell Therapy. *N Engl J. Med.* **2016**, *375* (26), 2561−2569.
(11) Quail, D. F.; Joyce, J. A. The Microenvironmental Landscape of Brain Tumors. *Cancer Cell* **2017**, *31* (3), 326−341.
(12) Ginhoux, F.; Greter, M.; Leboeuf, M.; Nandi, S.; See, P.; Gokhan, S.; Mehler, M. F.; Conway, S. J.; Ng, L. G.; Stanley, E. R.; Samokhvalov, I. M.; Merad, M. Fate Mapping Analysis Reveals That Adult Microglia Derive from Primitive Macrophages. *Science* **2010**, *330* (6005), 841−845.
(13) Gomez perdiguero, E.; Klapproth, K.; Schulz, C.; Busch, K.; Azzoni, E.; Crozet, L.; Garner, H.; Trouillet, C.; De bruijn, M. F.; Geissmann, F.; Rodewald, H.-R. Tissue-Resident Macrophages Originate from Yolk-Sac-Derived Erythro-Myeloid Progenitors. *Nature* **2015**, *518* (7540), 547−551.
(14) Hambardzumyan, D.; Gutmann, D. H.; Kettenmann, H. The Role of Microglia and Macrophages in Glioma Maintenance and Progression. *Nat. Neurosci* **2016**, *19* (1), 20−27.
(15) Mantovani, A.; Allavena, P.; Marchesi, F.; Garlanda, C. Macrophages as Tools and Targets in Cancer Therapy. *Nat. Rev. Drug Discov* **2022**, *21* (11), 799−820.
(16) Coniglio, S. J.; Eugenin, E.; Dobrenis, K.; Stanley, E. R.; West, B. L.; Symons, M. H.; Segall, J. E. Microglial Stimulation of Glioblastoma Invasion Involves Epidermal Growth Factor Receptor (EGFR) and Colony Stimulating Factor 1 Receptor (CSF-1R) Signaling. *Mol. Med.* **2012**, *18* (1), 519−527.
(17) Pyonteck, S. M.; Akkari, L.; Schuhmacher, A. J.; Bowman, R. L.; Sevenich, L.; Quail, D. F.; Olson, O. C.; Quick, M. L.; Huse, J. T.; Teijeiro, V.; Setty, M.; Leslie, C. S.; Oei, Y.; Pedraza, A.; Zhang, J.; Brennan, C. W.; Sutton, J. C.; Holland, E. C.; Daniel, D.; Joyce, J. A. CSF-1R Inhibition Alters Macrophage Polarization and Blocks Glioma Progression. *Nat. Med.* **2013**, *19* (10), 1264−1272.
(18) Denardo, D. G.; Ruffell, B. Macrophages as Regulators of Tumour Immunity and Immunotherapy. *Nat. Rev. Immunol* **2019**, *19* (6), 369−382.
(19) Roskoski, R. Properties of FDA-Approved Small Molecule Protein Kinase Inhibitors: A 2021 Update. *Pharmacol. Res.* **2021**, *165*, No. 105463.
(20) Stafford, J. H.; Hirai, T.; Deng, L.; Chernikova, S. B.; Urata, K.; West, B. L.; Brown, J. M. Colony Stimulating Factor 1 Receptor Inhibition Delays Recurrence of Glioblastoma after Radiation by Altering Myeloid Cell Recruitment and Polarization. *Neuro Oncol* **2016**, *18* (6), 797−806.
(21) Mok, S.; Koya, R. C.; Tsui, C.; Xu, J.; Robert, L.; Wu, L.; Graeber, T.; West, B. L.; Bollag, G.; Ribas, A. Inhibition of CSF-1 Receptor Improves the Antitumor Efficacy of Adoptive Cell Transfer Immunotherapy. *Cancer Res.* **2014**, *74* (1), 153−161.
(22) Butowski, N.; Colman, H.; De groot, J. F.; Omuro, A. M.; Nayak, L.; Wen, P. Y.; Cloughesy, T. F.; Marimuthu, A.; Haidar, S.; Perry, A.; Huse, J.; Phillips, J.; West, B. L.; Nolop, K. B.; Hsu, H. H.; Ligon, K. L.; Molinaro, A. M.; Prados, M. Orally Administered Colony Stimulating Factor 1 Receptor Inhibitor PLX3397 in Recurrent Glioblastoma: An Ivy Foundation Early Phase Clinical Trials Consortium Phase II Study. *Neuro Oncol* **2016**, *18* (4), 557−564.
(23) Kaur, B.; Khwaja, F. W.; Severson, E. A.; Matheny, S. L.; Brat, D. J.; Van meir, E. G. Hypoxia and the Hypoxia-Inducible-Factor Pathway in Glioma Growth and Angiogenesis. *Neuro Oncol* **2005**, *7* (2), 134−153.
(24) Boyd, N. H.; Tran, A. N.; Bernstock, J. D.; Etminan, T.; Jones, A. B.; Gillespie, G. Y.; Friedman, G. K.; Hjelmeland, A. B. Glioma Stem Cells and Their Roles within the Hypoxic Tumor Microenvironment. *Theranostics* **2021**, *11* (2), 665−683.
(25) Cheng, H.-B.; Zhang, S.; Qi, J.; Liang, X.-J.; Yoon, J. Advances in Application of Azobenzene as a Trigger in Biomedicine: Molecular Design and Spontaneous Assembly. *Adv. Mater.* **2021**, *33* (26), No. e2007290.
(26) Agard, N. J.; Prescher, J. A.; Bertozzi, C. R. A Strain-Promoted [3 + 2] Azide-Alkyne Cycloaddition for Covalent Modification of Biomolecules in Living Systems. *J. Am. Chem. Soc.* **2004**, *126* (46), 15046−15047.
(27) Heczey, A.; Liu, D.; Tian, G.; Courtney, A. N.; Wei, J.; Marinova, E.; Gao, X.; Guo, L.; Yvon, E.; Hicks, J.; Liu, H.; Dotti, G.; Metelitsa, L. S. Invariant NKT Cells with Chimeric Antigen Receptor Provide a Novel Platform for Safe and Effective Cancer Immunotherapy. *Blood* **2014**, *124* (18), 2824−2833.
(28) Mo, F.; Pellerino, A.; Soffietti, R.; Rudà, R. Blood-Brain Barrier in Brain Tumors: Biology and Clinical Relevance. *Int. J. Mol. Sci.* **2021**, *22* (23), 12654.
(29) Oberoi, R. K.; Parrish, K. E.; Sio, T. T.; Mittapalli, R. K.; Elmquist, W. F.; Sarkaria, J. N. Strategies to Improve Delivery of Anticancer Drugs across the Blood-Brain Barrier to Treat Glioblastoma. *Neuro Oncol* **2016**, *18* (1), 27−36.

https://doi.org/10.1021/acsnano.4c00050
ACS Nano XXXX, XXX, XXX−XXX

(30) Shergalis, A.; Bankhead, A.; Luesakul, U.; Muangsin, N.; Neamati, N. Current Challenges and Opportunities in Treating Glioblastoma. *Pharmacol Rev.* **2018**, *70* (3), 412−445.
(31) Louveau, A.; Smirnov, I.; Keyes, T. J.; Eccles, J. D.; Rouhani, S. J.; Peske, J. D.; Derecki, N. C.; Castle, D.; Mandell, J. W.; Lee, K. S.; Harris, T. H.; Kipnis, J. Structural and Functional Features of Central Nervous System Lymphatic Vessels. *Nature* **2015**, *523* (7560), 337−341.
(32) Castellani, G.; Croese, T.; Peralta ramos, J. M.; Schwartz, M. Transforming the Understanding of Brain Immunity. *Science* **2023**, *380* (6640), No. eabo7649.
(33) Schläger, C.; Körner, H.; Krueger, M.; Vidoli, S.; Haberl, M.; Mielke, D.; Brylla, E.; Issekutz, T.; Cabañas, C.; Nelson, P. J.; Ziemssen, T.; Rohde, V.; Bechmann, I.; Lodygin, D.; Odoardi, F.; Flügel, A. Effector T-Cell Trafficking between the Leptomeninges and the Cerebrospinal Fluid. *Nature* **2016**, *530* (7590), 349−353.
(34) Liu, Z.; Zhou, J.; Yang, X.; Liu, Y.; Zou, C.; Lv, W.; Chen, C.; Cheng, K. K.-Y.; Chen, T.; Chang, L.-J.; Wu, D.; Mao, J. Safety and Antitumor Activity of GD2-Specific 4SCAR-T Cells in Patients with Glioblastoma. *Mol. Cancer* **2023**, *22* (1), 3.
(35) Peng, J.; Yang, Q.; Shi, K.; Xiao, Y.; Wei, X.; Qian, Z. Intratumoral Fate of Functional Nanoparticles in Response to Microenvironment Factor: Implications on Cancer Diagnosis and Therapy. *Adv. Drug Deliver Rev.* **2019**, *143*, 37−67.
(36) Cersosimo, F.; Lonardi, S.; Ulivieri, C.; Martini, P.; Morrione, A.; Vermi, W.; Giordano, A.; Giurisato, E. CSF-1R in Cancer: More than a Myeloid Cell Receptor. *Cancers (Basel)* **2024**, *16* (2), 282.
(37) Sun, L.; Liang, H.; Yu, W.; Jin, X. Increased Invasive Phenotype of CSF-1R Expression in Glioma Cells via the ERK1/2 Signaling Pathway. *Cancer Gene Ther.* **2019**, *26* (5−6), 136−144.
(38) Christofides, A.; Strauss, L.; Yeo, A.; Cao, C.; Charest, A.; Boussiotis, V. A. The Complex Role of Tumor-Infiltrating Macrophages. *Nat. Immunol* **2022**, *23* (8), 1148−1156.
(39) Xia, Y.; Rao, L.; Yao, H.; Wang, Z.; Ning, P.; Chen, X. Engineering Macrophages for Cancer Immunotherapy and Drug Delivery. *Adv. Mater.* **2020**, *32* (40), No. e2002054.
(40) Verma, M.; Obergfell, K.; Topp, S.; Panier, V.; Wu, J. The Next-Generation CAR-T Therapy Landscape. *Nat. Rev. Drug Discov* **2023**, *22* (10), 776−777.
(41) Bagley, S. J.; Desai, A. S.; Linette, G. P.; June, C. H.; O'rourke, D. M. CAR T-Cell Therapy for Glioblastoma: Recent Clinical Advances and Future Challenges. *Neuro-Oncology* **2018**, *20* (11), 1429−1438.
(42) Preusser, M.; Lim, M.; Hafler, D. A.; Reardon, D. A.; Sampson, J. H. Prospects of Immune Checkpoint Modulators in the Treatment of Glioblastoma. *Nat. Rev. Neurol* **2015**, *11* (9), 504−514.
(43) Gomez, G. G.; Kruse, C. A. Mechanisms of Malignant Glioma Immune Resistance and Sources of Immunosuppression. *Gene Ther. Mol. Biol.* **2006**, *10* (A), 133−146.
(44) June, C. H.; O'connor, R. S.; Kawalekar, O. U.; Ghassemi, S.; Milone, M. C. CAR T Cell Immunotherapy for Human Cancer. *Science* **2018**, *359* (6382), 1361−1365.
(45) Sarkaria, J. N.; Hu, L. S.; Parney, I. F.; Pafundi, D. H.; Brinkmann, D. H.; Laack, N. N.; Giannini, C.; Burns, T. C.; Kizilbash, S. H.; Laramy, J. K.; Swanson, K. R.; Kaufmann, T. J.; Brown, P. D.; Agar, N. Y. R.; Galanis, E.; Buckner, J. C.; Elmquist, W. F. Is the Blood-Brain Barrier Really Disrupted in All Glioblastomas? A Critical Assessment of Existing Clinical Data. *Neuro Oncol* **2018**, *20* (2), 184−191.
(46) Goff, S. L.; Morgan, R. A.; Yang, J. C.; Sherry, R. M.; Robbins, P. F.; Restifo, N. P.; Feldman, S. A.; Lu, Y.-C.; Lu, L.; Zheng, Z.; Xi, L.; Epstein, M.; Mcintyre, L. S.; Malekzadeh, P.; Raffeld, M.; Fine, H. A.; Rosenberg, S. A. Pilot Trial of Adoptive Transfer of Chimeric Antigen Receptor-Transduced T Cells Targeting EGFRvIII in Patients With Glioblastoma. *J. Immunother* **2019**, *42* (4), 126−135.
(47) Brown, C. E.; Badie, B.; Barish, M. E.; Weng, L.; Ostberg, J. R.; Chang, W.-C.; Naranjo, A.; Starr, R.; Wagner, J.; Wright, C.; Zhai, Y.; Bading, J. R.; Ressler, J. A.; Portnow, J.; D'apuzzo, M.; Forman, S. J.; Jensen, M. C. Bioactivity and Safety of IL13Rα2-Redirected Chimeric Antigen Receptor CD8+ T Cells in Patients with Recurrent Glioblastoma. *Clin. Cancer Res.* **2015**, *21* (18), 4062−4072.
(48) Agliardi, G.; Liuzzi, A. R.; Hotblack, A.; De feo, D.; Núñez, N.; Stowe, C. L.; Friebel, E.; Nannini, F.; Rindlisbacher, L.; Roberts, T. A.; Ramasawmy, R.; Williams, I. P.; Siow, B. M.; Lythgoe, M. F.; Kalber, T. L.; Quezada, S. A.; Pule, M. A.; Tugues, S.; Straathof, K.; Becher, B. Intratumoral IL-12 Delivery Empowers CAR-T Cell Immunotherapy in a Pre-Clinical Model of Glioblastoma. *Nat. Commun.* **2021**, *12* (1), 444.
(49) Alizadeh, D.; Wong, R. A.; Yang, X.; Wang, D.; Pecoraro, J. R.; Kuo, C.-F.; Aguilar, B.; Qi, Y.; Ann, D. K.; Starr, R.; Urak, R.; Wang, X.; Forman, S. J.; Brown, C. E. IL15 Enhances CAR-T Cell Antitumor Activity by Reducing mTORC1 Activity and Preserving Their Stem Cell Memory Phenotype. *Cancer Immunol Res.* **2019**, *7* (5), 759−772.
(50) Shen, S. H.; Woroniecka, K.; Barbour, A. B.; Fecci, P. E.; Sanchez-perez, L.; Sampson, J. H. CAR T Cells and Checkpoint Inhibition for the Treatment of Glioblastoma. *Expert Opin Biol. Ther* **2020**, *20* (6), 579−591.
(51) Chalise, L.; Kato, A.; Ohno, M.; Maeda, S.; Yamamichi, A.; Kuramitsu, S.; Shiina, S.; Takahashi, H.; Ozone, S.; Yamaguchi, J.; Kato, Y.; Rockenbach, Y.; Natsume, A.; Todo, T. Efficacy of Cancer-Specific Anti-Podoplanin CAR-T Cells and Oncolytic Herpes Virus G47Δ Combination Therapy against Glioblastoma. *Mol. Ther Oncolytics* **2022**, *26*, 265−274.
(52) Song, Y.; Liu, Q.; Zuo, T.; Wei, G.; Jiao, S. Combined Antitumor Effects of Anti-EGFR Variant III CAR-T Cell Therapy and PD-1 Checkpoint Blockade on Glioblastoma in Mouse Model. *Cell Immunol* **2020**, *352*, No. 104112.
(53) Chmielewski, M.; Abken, H. CAR T Cells Transform to Trucks: Chimeric Antigen Receptor-Redirected T Cells Engineered to Deliver Inducible IL-12 Modulate the Tumour Stroma to Combat Cancer. *Cancer Immunol Immunother* **2012**, *61* (8), 1269−1277.
(54) Johnson, D. B.; Nebhan, C. A.; Moslehi, J. J.; Balko, J. M. Immune-Checkpoint Inhibitors: Long-Term Implications of Toxicity. *Nat. Rev. Clin Oncol* **2022**, *19* (4), 254−267.
(55) Koneru, M.; O'cearbhaill, R.; Pendharkar, S.; Spriggs, D. R.; Brentjens, R. J. A Phase I Clinical Trial of Adoptive T Cell Therapy Using IL-12 Secreting MUC-16(Ecto) Directed Chimeric Antigen Receptors for Recurrent Ovarian Cancer. *J. Transl. Med.* **2015**, *13*, 102.
(56) Craddock, J. A.; Lu, A.; Bear, A.; Pule, M.; Brenner, M. K.; Rooney, C. M.; Foster, A. E. Enhanced Tumor Trafficking of GD2 Chimeric Antigen Receptor T Cells by Expression of the Chemokine Receptor CCR2b. *J. Immunother* **2010**, *33* (8), 780−788.
(57) Di stasi, A.; De angelis, B.; Rooney, C. M.; Zhang, L.; Mahendravada, A.; Foster, A. E.; Heslop, H. E.; Brenner, M. K.; Dotti, G.; Savoldo, B. T Lymphocytes Coexpressing CCR4 and a Chimeric Antigen Receptor Targeting CD30 Have Improved Homing and Antitumor Activity in a Hodgkin Tumor Model. *Blood* **2009**, *113* (25), 6392−6402.
(58) Tang, L.; Zheng, Y.; Melo, M. B.; Mabardi, L.; Castaño, A. P.; Xie, Y.-Q.; Li, N.; Kudchodkar, S. B.; Wong, H. C.; Jeng, E. K.; Maus, M. V.; Irvine, D. J. Enhancing T Cell Therapy through TCR-Signaling-Responsive Nanoparticle Drug Delivery. *Nat. Biotechnol.* **2018**, *36* (8), 707−716.
(59) Siriwon, N.; Kim, Y. J.; Siegler, E.; Chen, X.; Rohrs, J. A.; Liu, Y.; Wang, P. CAR-T Cells Surface-Engineered with Drug-Encapsulated Nanoparticles Can Ameliorate Intratumoral T-Cell Hypofunction. *Cancer Immunol Res.* **2018**, *6* (7), 812−824.
(60) Hao, M.; Hou, S.; Li, W.; Li, K.; Xue, L.; Hu, Q.; Zhu, L.; Chen, Y.; Sun, H.; Ju, C.; Zhang, C. Combination of Metabolic Intervention and T Cell Therapy Enhances Solid Tumor Immunotherapy. *Sci. Transl. Med.* **2020**, *12* (571), No. eaaz6667.
(61) Bikfalvi, A.; Costa, C. A. da; Avril, T.; Barnier, J.-V.; Bauchet, L.; Brisson, L.; Cartron, P. F.; Castel, H.; Chevet, E.; Chneiweiss, H.; Clavreul, A.; Constantin, B.; Coronas, V.; Daubon, T.; Dontenwill, M.; Ducray, F.; Entz-werlé, N.; Figarella-branger, D.; Fournier, I.; Frenel, J.-S.; Gabut, M.; Galli, T.; Gavard, J.; Huberfeld, G.; Hugnot, J.-P.; Idbaih, A.; Junier, M.-P.; Mathivet, T.; Menei, P.; Meyronet, D.;

https://doi.org/10.1021/acsnano.4c00050
ACS Nano XXXX, XXX, XXX−XXX

Mirjolet, C.; Morin, F.; Mosser, J.; Moyal, E. C.-J.; Rousseau, V.; Salzet, M.; Sanson, M.; Seano, G.; Tabouret, E.; Tchoghandjian, A.; Turchi, L.; Vallette, F. M.; Vats, S.; Verreault, M.; Virolle, T. Challenges in Glioblastoma Research: Focus on the Tumor Microenvironment. *Trends Cancer* **2023**, *9* (1), 9−27.
(62) Pittet, M. J.; Michielin, O.; Migliorini, D. Clinical Relevance of Tumour-Associated Macrophages. *Nat. Rev. Clin Oncol* **2022**, *19* (6), 402−421.
(63) Ml, B.; Sln, M.; Er, A.; Tr, M.; Am, K.; Xo, B. Multidimensional Communication in the Microenvirons of Glioblastoma. *Nat. Rev. Neurol.* **2018**, *14* (8), 482−495.
(64) Yan, D.; Kowal, J.; Akkari, L.; Schuhmacher, A. J.; Huse, J. T.; West, B. L.; Joyce, J. A. Inhibition of Colony Stimulating Factor-1 Receptor Abrogates Microenvironment-Mediated Therapeutic Resistance in Gliomas. *Oncogene* **2017**, *36* (43), 6049−6058.
(65) Diehl, K. L.; Kolesnichenko, I. V.; Robotham, S. A.; Bachman, J. L.; Zhong, Y.; Brodbelt, J. S.; Anslyn, E. V. Click and Chemically Triggered Declick Reactions through Reversible Amine and Thiol Coupling via a Conjugate Acceptor. *Nature Chem.* **2016**, *8* (10), 968−973.
(66) Liu, B.; Wu, R.; Gong, S.; Xiao, H.; Thayumanavan, S. In Situ Formation of Polymeric Nanoassemblies Using an Efficient Reversible Click Reaction. *Angew. Chem., Int. Ed. Engl.* **2020**, *59* (35), 15135−15140.

https://doi.org/10.1021/acsnano.4c00050
ACS Nano XXXX, XXX, XXX−XXX